

Spectral quantification of nonlinear behaviour of the nearshore seabed and correlations with potential forcings at Duck, N.C., U.S.A.

Magar, V.^{a,*}, Lefranc, M.^b, Hoyle, R. B.^c, Reeve, D. E.^a

^a*Coastal Engineering Research Group, Marine Institute, School of Marine Science and Engineering, University of Plymouth, Drake Circus, Plymouth PL48AA. Tel: +44 (0)1752 586137, Fax: +44 (0)1752 232638*

^b*Laboratoire de Physique des Lasers, Atomes, Molécules (PhLAM) and Centre d' Études et de Recherches Lasers et Applications (CERLA), UFR de Physique, Bat. P5, Université des Sciences et Technologies de Lille, F-59655 Villeneuve d'Ascq CEDEX, France*

^c*Department of Mathematics, University of Surrey, Guildford, Surrey, GU2 7XH, UK*

Abstract

Local bathymetric quasi-periodic patterns of oscillation are identified from monthly profile surveys taken at two shore-perpendicular transects at the USACE field research facility in Duck, North Carolina, USA, spanning 24.5 years and covering the swash and surf zones. The chosen transects are the two furthest (north and south) from the pier located at the study site. Research at Duck has traditionally focused on one or more of these transects as the effects of the pier are least at these locations. The patterns are identified using singular spectrum analysis (SSA). Possible correlations with potential forcing mechanisms are discussed by 1) doing an SSA with same parameter settings to independently identify the quasi-periodic cycles embedded within three potentially linked sequences: monthly wave heights (MWH), monthly mean water levels (MWL) and the large scale atmospheric index known as the North Atlantic Oscillation (NAO) and 2) comparing the patterns within MWH, MWL and NAO to the local bathymetric patterns. The results agree well with previous patterns identified using wavelets and confirm the highly

*Corresponding author

Email addresses: vmagar@plymouth.ac.uk (Magar, V.), marc.lefranc@univ-lille1.fr (Lefranc, M.), R.Hoyle@surrey.ac.uk (Hoyle, R. B.), dominic.reeve@plymouth.ac.uk (Reeve, D. E.)

nonstationary behaviour of beach levels at Duck; the discussion of potential correlations with hydrodynamic and atmospheric phenomena is a new contribution. The study is then extended to all measured bathymetric profiles, covering an area of 1100m (alongshore) by 440m (cross-shore), to 1) analyse linear correlations between the bathymetry and the potential forcings using multivariate empirical orthogonal functions (MEOF) and linear correlation analysis and 2) identify which collective quasi-periodic bathymetric patterns are correlated with those within MWH, MWL or NAO, based on a (nonlinear) multichannel singular spectrum analysis (MSSA). MEOF and linear correlation analysis are equivalent, with spatial distributions of the linear correlation coefficient between bathymetry and the potential forcing being the same as those of the relevant EOF. Regions of high correlations are supported by what would be expected from knowledge about local physical processes. At the two transects furthest from the pier, regions with high correlation and anti-correlation broadly agree with the SSA findings. The MEOF/correlation analysis was used as a preliminary step towards the identification of collective spatio-temporal patterns between all bathymetric profiles and the potential forcings. This final analysis, based on MSSA, showed that no collective interannual patterns of oscillations are present throughout the bathymetry and the three potential forcings - which was to be expected as SSA showed the highly localised nature of the interannual bathymetric patterns. Also, annual and semi-annual cycles within the bathymetry are strongly correlated to the monthly wave height, in agreement with the SSA findings. Other collective intra-annual cycles besides the semi-annual were identified; they were all correlated to the NAO.

Key words: Sandy beaches, Beach features, Coastal morphology, Spectral analysis, Oscillations, Duck

1. Introduction

Understanding the evolution of beaches in the long term (at yearly to decadal time scales) poses an important challenge to researchers. This is because it is unclear how the mechanisms forcing the morphology, such as hydrodynamic and sediment transport processes, affect beaches at such time scales (Southgate et al., 2003; Dodd et al., 2003), and also because datasets from which yearly to decadal patterns of behaviour may be extracted are at present scarce. Because of the threat of climate change, improved un-

derstanding and better predictive tools are crucial, both for researchers and end-users alike.

The term 'coastal morphodynamics' has been coined to describe the investigation of changes in the shape (or morphology) of coastal features such as beaches, sandbanks and so on. There are several modelling approaches adopted in coastal morphodynamics, for instance sequential models, equilibrium models, equation-based or data-based models. In long-term morphodynamical modelling data-based approaches tend to be preferred because of the difficulties in assessing how the different processes affect the dynamics in the long-term, as was mentioned above. Equilibrium-based models of sandbar systems assume sandbar migration towards a wave height dependent equilibrium location (see, e.g. Plant et al., 1999). Sequential models either analyse single cross-shore profiles or incorporate longshore variability; in the former the aim is an analysis of cross-shore sediment transport, in particular the characterisation of cyclic patterns, while in the latter the aim consists of identifying morphological beach states that would characterise morphological sequences and thus help understand and classify nearshore bars in terms of their shape and dynamics (Wright and Short, 1984; Lippmann and Holman, 1990). An important aspect of sandbar dynamics is the observed interactions between sandbars when several bars are present. At Duck, such interactions have been studied by Lippmann et al. (1993), who observed significant non-linear behaviour of inner bars when outer bars were present.

There are two possible signal selection criteria used to analyse nearshore morphodynamics. One is to analyse spatial patterns, for instance the evolution of the sandbar crests and troughs or the evolution of the shoreline, and the other is to find patterns optimizing a statistical measure, for instance patterns identified with empirical orthogonal functions (EOFs), Canonical Correlation Analysis (CCA) or wavelet analysis. The spatial pattern approach has been extremely popular and has contributed significantly to the understanding of sandbar dynamics (see Lippmann and Holman, 1990; Lippmann et al., 1993; Wijnberg and Terwindt, 1995; Plant et al., 1999; Wijnberg and Kroon, 2002; Różyński, 2003; Kuriyama et al., 2008; Pape and Ruessink, 2008, and references therein). These studies focus on descriptions of bar migration, bar amplitude evolution and development of bar asymmetry. Using an optimal statistical measure as a pattern identification criterion has also been very popular; these methods are particularly useful for temporal or spatio-temporal pattern analysis. For instance, EOFs identify the linear modes of maximal variance, while CCA leads to linear modes that maximize

the correlations between two time series. CCA has been used recently at Duck to analyse correlations between wave climate and bathymetric evolution at Duck, with reasonable success (Larson and Kraus, 1994; Horrillo-Caraballo and Reeve, 2008). Reeve et al. (2008), on the other hand, used wavelets to analyse dominant temporal patterns of behaviour at a cross-shore transect in Duck. In some cases, it has been possible to link the spatial patterns to the patterns optimizing a statistical measure (see, e.g., Lippmann et al., 1993; Wijnberg and Terwindt, 1995); in others the interpretation of the patterns optimizing a statistical measure may be less obvious, for instance for the 1-2 yearly temporal patterns embedded in the seabed dynamics at Duck, identified by Reeve et al. (2008), in which case additional analyses may be necessary to assess their origin.

We postulate that different bathymetric regions have different nonlinear behaviour depending on their cross-shore and longshore location, and that several of the observed patterns are well correlated with patterns embedded within potential forcing mechanisms such as the monthly wave patterns, monthly sea level patterns or the NAO. Hence, nonlinear patterns of behaviour of bed levels at Duck will be quantified using singular spectrum analysis (SSA) and spectral density analysis SDA to characterise quasi-periodic oscillations. Possible correlations between these patterns and those embedded within large-scale phenomena that might potentially be at the origin of the observed behaviour will be discussed, and correlations between them will be confirmed by further multivariate EOF (MEOF) and multichannel singular spectrum analysis (MSSA) studies.

SSA and MSSA are two data-based, nonlinear methods that optimize modes of maximal variance. The methods are applied to time-lagged copies of bathymetric (and hydrodynamic or atmospheric index) time series and were chosen because they are good at identifying underlying temporal and spatio-temporal patterns of oscillation even when the data is short and noisy (Vautard and Ghil, 1989), as is the case for most coastal morphodynamics datasets. Vautard and Ghil (1989) have shown, for instance, that SSA is capable of describing the dynamics of paleoclimatic oscillations obtained from marine sediment core measurements that had as few as 184 data points, as well as the statistically significant number of degrees of freedom. There are other measures of dimension aside from the number of degrees of freedom of a dynamical system, such as the correlation dimension, which is a measure of the dimensionality of the space occupied by a set of points. However, Grassberger (1986) and Vautard and Ghil (1989) have showed that reliable

correlation dimension computations for the same core measurements were not possible due to the data's shortness and noisiness. Indeed, it is well known that in general the number of data points needed for accurate computation of the correlation dimension would be much larger, more likely in the order of a thousand or larger (Grassberger and Procaccia, 1983; Ruelle, 1990). When analysing temporal patterns, however, it is important as well that the frequency of sampling is significantly larger than the frequency of the studied pattern, regardless of the size of the dataset (Gilmore and Lefranc, 2002). For our purposes SSA (and by extension MSSA) is a perfectly suitable technique since our interest focuses on the quasi-oscillations underlying the dynamics and these oscillations are well captured by such techniques.

SSA has some similarities with empirical orthogonal functions (EOF), first applied to analysing beach variation by Winant et al. (1975). Both SSA and EOF, as well as MSSA and Complex EOF (CEOF), have very recently been exploited to analyse long-term sea level changes (Papadopoulos and Tsimplis, 2006), as well as behavioural patterns in coastal features such as shorelines (Różyński et al., 2001; Southgate et al., 2003; Różyński, 2005; Miller and Dean, 2006) and nearshore sandbars (Wijnberg and Terwindt, 1995; Rattan et al., 2005). SSA may be used together with spectral density analysis (SDA) to characterise the frequencies identified with SSA. However, one major benefit of SSA over spectral analysis is that, just as with wavelet analysis, SSA is capable of capturing nonstationarity in patterns (Li et al., 2005; Reeve et al., 2007).

Southgate et al. (2003) used SSA to identify the long-term trend of the shoreline at Duck, between 1980 and 1993. The authors analysed the component of the signal resolved by the first three eigenvalues. Their reconstruction showed no evidence of quasi-periodic oscillations of the shoreline. Rather, it led to the identification of an accretional trend from 1981 to 1990, followed by significant erosion from 1990 onwards. This contrasted with their findings at Ogata beach, Japan, where a clear linear trend of erosion, with a 5-yearly cycle superimposed, could be identified.

As Różyński et al. (2001) indicate, the specification of what is a signal and what is noise is crucial in SSA. These authors have used this technique to analyse shoreline evolution at Lubiatowo, Poland, between 1983 and 1999. Three long-term patterns were identified, with periods of 9, 16 or 32 years, at different positions along the coastline. Interannual cycles of 2-3 and 3-4 years were also found. Significant variability occurred at some positions, however. This study also pointed to the possible existence of chaotic be-

haviour as resolved by the second eigenvalue, which the authors linked to a response to extreme events. An association between the rhythmicity of the bed level variations and sand bar propagation was also postulated, supported by the existence of high correlations between shoreline positions and the inner bar crests (Pruszek et al., 1999). The authors also explain some findings in terms of self-organisation. While the implementation of EOF is relatively straightforward, with SSA intermediate computations and tests are necessary to obtain a set of uncorrelated reconstructed components and avoid misinterpretations. However, SSA is superior to EOF because it can identify nonlinear, temporal patterns underlying the dynamics, while EOF is a linear method which cannot identify nonlinear patterns at all. MSSA follows the same principles as SSA, but is performed on a vector that contains variations at different positions rather than at a single location. Thus, MSSA is more likely to identify collective patterns of behaviour. MSSA is sometimes called multivariate extended empirical orthogonal function (MEEOF) analysis (Mote et al., 2000).

MSSA has been applied to Lubiato, to identify the collective patterns of behaviour of the shoreline (Różyński, 2005). However, such patterns will necessarily appear as well in the SSA at individual positions, but possibly not everywhere as the dominant patterns of behaviour. At Lubiato, three collective quasi-periodic oscillations were identified, with periods of 7 to 8 years, 20 years and several decades. The authors commented that the 7 to 8-yearly cycle might be forced by the North Atlantic Oscillation (NAO), which has an important influence in the Baltic Sea. Very recently, (Różyński, 2010) extended his analysis and found supporting evidence that the NAO may affect the bathymetry through a gentle coupling between the NAO, the hydrodynamics and the seabed.

As indicated by Falques et al. (2000), the spatial regularity of nearshore patterns implies that nearshore dynamics may be understood and, most importantly, described using simple physical mechanisms. That we need to look for mechanisms acting in the long term is particularly important. Within the surf zone and at the shore, the occurrence of spatially rhythmic patterns has been attributed to the presence of low-frequency waves, such as infragravity waves (Bowen and Guza, 1978; Bowen, 1980; Holman and Bowen, 1982). However, infragravity waves are responsible for the short term response of some beaches, not the interannual behaviour. At such large time scales the wave-related parameter that is of importance is the monthly averaged wave height. Note that we are not implying there ought to be a simple relationship

between the waves and the bathymetry, whose response to forcings has been shown to be nonlinear in other studies (Falques et al., 2000, and references therein). This nonlinearity could be reflected in the difference between amplitudes and phases, as well as in the characteristics of the regime changes observed in the corresponding time series. In the case of longshore parallel bars, the bar crests and troughs may cause redistribution of wave energy, variations in the wave breaking point and wave transformation processes (i.e. wave refraction, reflection and diffraction) which in turn, produce a radiation stress which is no longer in equilibrium with the set-up and set-down, hence creating a steady circulation (Falques et al., 2000). Cellular automata models have been developed to analyse free evolution of the seabed (Coco et al., 1999), while nonlinear morphodynamic evolution models have permitted the analysis of difference in bed response depending on an initial perturbation (see, e.g., Klein and Schuttelaars, 2006). Aside from the monthly averaged wave heights and atmospheric phenomena such as NAO, it is likely that the tides and storm surges also have an effect on long term morphodynamics. Tides are fully predictable shallow water waves generated by gravitational forces between the Earth, the Sun and the Moon. Storm surges change the water depth through pressure forces, wind stresses and wave set-up and set-down, and this in turn changes the water depth at the bar crests and troughs, and hence the radiation stresses mentioned above. Given that tides and storm surges may be combined in one single parameter, namely the mean water level, some of the patterns observed in the bathymetric evolution may potentially be correlated with patterns found within a water level time series.

In Sect. 2 below the case study data is presented and the SSA and SDA techniques are explained in more detail, together with the MEOF and the MSSA. The results are presented in Sect. 3 and they are then discussed in Sect 4. Sensitivity to window length changes is discussed in Sect. 4.1. Comparisons with previous investigations are presented in Sect. 4.2. In Sect. 4.3, SSA and SDA of the monthly averaged wave heights at a nearshore wave gauge are performed and the patterns are compared to those of the bathymetry, together with similar analyses for the North Atlantic Oscillation (taken as an average over the whole area of study) to illustrate the possible correlations with large-scale phenomena. Sect. 4.4 discusses linear correlations between the full set of bathymetric measurements and the monthly mean wave heights, monthly mean sea level and monthly NAO. Coherent spatio-temporal correlations identified via MSSA are also discussed. Finally, Sect. 5 contains a summary and some concluding remarks. Websites are re-

ferred to as data or software sources, when appropriate, in accordance with copyright requirements.

2. Summary of data and techniques

2.1. The source and nature of the data under analysis

Data were provided by the Field Research Facility (FRF), Field Data Collections and Analysis Branch, US Army Corps of Engineers (USACE), Duck, N. C., available from <http://www.frf.usace.army.mil>. The site consists of an open straight beach characterized by relatively regular, shore parallel contours with a barred surf zone and a moderate slope; these characteristics change close to a pier by the FRF facility that extends from the dune to a nominal water depth of approximately 7 m. The site has been comprehensively described by previous authors (Howd and Birkemeier, 1987; Lee and Birkemeier, 1993; Lee et al., 1998; Nicholls et al., 1998) and has also been the subject of numerous other studies (see introduction).

Measurements have been taken since June 1981 on a monthly basis over a series of 26 shore perpendicular transects, generally extending from the dune to approximately 950 m offshore, except for 4 lines, located at approximately 500 and 600 metres north and south of the pier, which have been surveyed every fortnight. Table 1 shows the averaged alongshore locations of these 4 lines with their associated measurement errors as well as their transect number (FRF location code). Note that the alongshore coordinate is assumed to be y and the cross-shore coordinate is x . The baseline is a shore parallel line with its origin at the South-East corner of the FRF property. On-going quality control and early publication of the surveys for those transects led to a significant number of studies based on them (see introduction). Moreover, the bathymetric evolution at these profiles is the least affected by the presence of the pier (Nicholls et al., 1998). However, important differences in the behaviour north and south of the pier, in particular regarding the sandbar system, have been observed (Shand et al., 1999).

Duck is an example of a net offshore bar migration (NOM) system, or a system with interannual cyclic sandbar behaviour (Shand et al., 1999; Ruessink and Terwindt, 2000). NOM is a cyclic phenomenon consisting of three stages (Ruessink and Kroon, 1994): bar generation near the shoreline (stage 1); systematic offshore migration of the bar across the surf zone during high energy periods (stage 2) and; disappearance of the bar in the outer surf zone (stage 3). Sandbar formation and migration may also be triggered

by previous profile geometries, with the degeneration of an outer bar often leading to formation of a new bar near the shoreline (Ruessink and Terwindt, 2000). NOM systems are often alongshore coherent, but at Duck this coherence is somewhat broken by the presence of the pier. Profiles at Duck vary from unbarred to triple barred, with the most common profile configuration being a double bar system consisting of a narrow inner bar and a broad outer bar (Howd and Birkemeier, 1987; Lee and Birkemeier, 1993; Lee et al., 1998).

Three parameters may characterise a NOM cycle at each stage: the average cross-shore distance over which bars migrate; the average duration of the bar migration and; the average return period of migration cycles. These parameters are site specific and in Duck they vary North and South of the pier. Shand et al. (1999, Fig. 7) summarise site parameter characteristics for a number of NOM systems including Duck North (DN) and Duck South (DS). While the total distance and the total duration of bar migration are relatively similar at DN and DS, the average return period is significantly different. The total distance travelled by the bars is 289.6 and 289.1 metres and their total duration (adding all three stages) is of 4.4 years and 4.1 years at DS and DN, respectively. However, for stage 2 for instance, the most active stage, the return period at DS is 3.2 years while at DN it is 6.8 years. The sand is transported back to the shoreline during fairweather periods through a variety of mechanisms: in the outer surf zone transport is driven by wave asymmetry while in the inner surf zone it also occurs through migrating bodies such as transverse bars or bar bifurcates generated during bar splitting processes (Holman and Sallenger, 1986; Holman and Lippmann, 1987; Lee et al., 1998; Shand, 2007). Since the wave climate has a very strong seasonal pattern with storms occurring mostly during the winter, annual patterns are expected to appear within the bathymetry.

In this study, the two outermost transects, i.e. transects 58 (Duck North) and 190 (Duck South), were first chosen to analyse the local quasi-oscillations embedded in the most active part of the surf zone. This reduced the cross-shore range to 390 m, between $x = 100$ and $x = 490$; this range coincided with that analysed by Southgate and Möller (2000) and includes most of the NOM width, that is, the region of sandbar migration (see Lee et al., 1998, Fig. 3). However the study area was extended to $x = 80$ m (to include the shoreline processes in more detail) and to $x = 520$ m (to check the type and strength of the correlations further offshore) for the linear correlation and MSSA analyses.] A spatial and temporal Akima interpolation (Akima, 1970) was performed on the data to obtain depth values at constant 10 m

intervals and at even timesteps of 30 days. These time and space interpolation intervals were also chosen by Southgate and Möller (2000) and prevent over-interpolation of the data. This procedure led to a 299-point time series at every bathymetric position, spanning from July 1981 to January 2006. Cross-shore bathymetric anomalies (with respect to the time-average at each position along the transect) are shown in Figs (a,i) and (b,i) within Fig. 1 for transects 58 and 190, respectively.

2.2. Methods used for local pattern analysis

Two complementary methods were used to identify local patterns of behaviour: Singular Spectrum Analysis (SSA) and Spectral Density Analysis (SDA). Both methods are described in detail in Appendix A.1 so here we only present a brief summary of SSA. Essentially, SSA is a nonlinear eigenvalue problem for a M -dimensional sequence $Z_n = (z_n, z_{n+1}, \dots, z_{n+M-1})$, for $n = 1, 2, \dots, N - M + 1$, of time-lagged copies of the bed level $z(t)$, at times $t = i\tau_s$, $i = 1, 2, \dots, N$, N being the length of the time series, τ_s the sampling interval and $M < N$ is the window length. Time scales of the dynamics that can be reconstructed from this time series are between τ_s and the window time span. Reconstructed components (RCs), linked to the eigenvalues of Z_n , have the same time span as the original time series and isolate one or more or the quasi-oscillatory patterns (depending on the number of eigenvalues used for the reconstruction). In this way, the signal was separated into a trend and a detrended signal using a window length, M , of 4 years. The trend corresponds to linear variations as well as patterns with periods above 3 to 5 years and is the RC of the first few eigenvalues of the SSA with $M = 4$. The trend can be analysed further with an SSA with window length of, say, 9 years, to identify long-period oscillations (LPOs) embedded within the trend signal. The detrended signal, on the other hand, contains short-period oscillations (SPOs), of periodicities of less than 5 years. Again, the periodicities of the SPOs can be determined with a further SSA on the detrended part of the signal. Note the overlap between LPOs and SPOs; this is due to the chosen window length of 4 years for the initial SSA. The robustness of the observations to small changes in the window length will be discussed in more detail further on.

Patterns embedded within monthly mean wave heights (MWH), monthly mean water levels (MWL) and the monthly North Atlantic Oscillation (NAO) were also extracted following the same procedure. The details of the hydrodynamic and atmospheric data are discussed in Appendix A.1. The patterns

obtained were compared to those within the bathymetry to identify locations where similar patterns are observed. This led to an evaluation of correlations between bathymetric and hydrodynamic/atmospheric patterns. Note that SSA would give a nonlinear measure of the correlations. Linear correlations were found as a preliminary step for in the analysis of spatio-temporal patterns of behaviour; the correlation analysis and the methods involved in the spatio-temporal study are introduced in the next section.

2.3. Correlation analysis and spatio-temporal patterns between bathymetry and potential forcings

Spatio-temporal collective bedlevel patterns were then analysed, not only on Transects 58 and 190 as before but also for all bathymetric surveys between them. A linear correlation analysis was first performed, by computing the correlation coefficient matrix, r , between the bedlevel time series and that of each of the potential forcings. This led to three different correlation coefficient matrices, one for the correlations of the bathymetry with the NAO, one for correlations with the MWH and one for correlations with the MWL, respectively. The values in r can be used to produce correlation coefficient contours to identify locations where the correlation between the bedlevels and the forcing is strongest. This analysis is intrinsically linked with the MEOF analysis carried out as a preliminary step for MSSA for all the bathymetry transects, because the correlation coefficient is equivalent to the covariance matrix, C , normalised by the square root of the product of the covariance at the associated diagonal elements:

$$r(i, j) = \frac{C(i, j)}{\sqrt{C(i, i)C(j, j)}},$$

and MEOF is based on the covariance of the multivariate matrix. The MEOF method is described in detail in Sect. A.2 within the Appendix. MEOF permits reduction in the number of channels from 1128 (one channel for each bathymetric location and one channel for each of the three potential forcings evaluated at a single location - see the Appendix for details) to three channels corresponding to the MEOF PCs in directions of maximal variance of the potential forcings (see Table A.3), with EOF1 corresponding to NAO, EOF2 to the mean wave heights (MWH) and EOF3 to the mean water levels (MWL). This reduction from 1128 to 3 channels is called a prefiltering. The system of 3 channels is then analysed with MSSA to identify which collective,

bedlevel spatio-temporal patterns may be correlated with NAO, MWH or MWL. The MSSA technique is described in Sec A.3 in the Appendix.

3. Results

3.1. Identification of trend and detrended signals

The trends, shown in Figs. 1(a,ii) and 1(b,ii) for transects 58 and 190, respectively, capture well the dominant patterns observed in Figs. 1(a,i) and 1(b,i), which seem to correspond to the extrema in the bathymetry and therefore are likely to correspond to the sandbars extrema. This is supported by the fact that some of the travelling characteristics of the sandbars have also been captured, because the extrema as well as surrounding bathymetric contours seem to travel offshore as time progresses.

For Transect 58, the patterns extracted resolve approximately 50% of the variance in regions where the extrema are well resolved. At other locations, such as between 130 and 220 m offshore, the variance resolved by the trend is slightly smaller than 50%. However, these results indicate that the trend and the detrended signal are equally important because they resolve an equal proportion of the total variance, and hence both should be analysed further.

For Transect 190, the results are very similar, i.e. the variance resolved by the trend and the detrended signals is about the same, though with the trend accounting for slightly less than 50% of the variance in this case, and so both signals need to be analysed. As with transect 58, the detrended signal, which contains the higher frequency oscillations (with periods generally below 4 years), seems to resolve slightly more of the variance between 130 and 220 m offshore.

The periods of the underlying cycle were computed all along transects 58 and 190; Table 2 shows the results at selected locations along the profiles. The uncertainties in the periods were estimated from figures of the power spectrum as well as from the uncertainty of the power values at each frequency. An example of a power spectrum is shown in Fig. 3, corresponding to position $x = 160$ m at transect 58. If the uncertainty interval of the power value extends to or beyond the peak power value, then the uncertainty of the position of the peak also extends to the frequency at that power value.

3.2. Identification of underlying quasi-oscillations

Long period oscillations (LPOs) and short period oscillations (SPOs) - with periods above and below 4 years, respectively - were then extracted

from the trend and the detrended time series. The RCs obtained when combining all the LPOs are shown in Figs. 2(a) and 2(c) for transects 58 and 190, respectively while the SPOs are shown in Figs. 2(b) and 2(d).

In relation to the LPOs, it is clear that these patterns have an important contribution below 350 to 400 m offshore, because the variance resolved by these patterns - shown in the upper plot of Figs. 2(a) and 2(c) - typically takes large values there. At both transects the signal contains roughly three regions where quasi-oscillations are important. At transect 58 these regions extend between $x = 130$ and 140 m, $x = 210$ and 260 m and $x = 340$ and 350 m; at transect 190, they extend between $x = 130$ and 180 m, $x = 230$ and 240 m and $x = 290$ to 370 m. Hence there is agreement in the number of regions but their extent differs. The main periods of the quasi-oscillatory patterns are summarised in Table 2. The table shows there is a lot of variability in the periods of the patterns, however, between 220 and 370 m offshore the periods of the patterns are close to those found within the NAO.

The SPOs, in contrast, may have an important contribution throughout the region under consideration, as the variance they resolve - see upper plots in Figs. 2(b) and 2(d) - is usually around 50%. Based on the information in Fig. 2(b) and Table 2, at transect 58 the signal contains a very clear yearly cycle in the region between $x = 100$ and 300 m. A 1 to 2-yearly cycle is also present between 200 and 300 m offshore. From $x = 300$ m onwards, the SPOs have periods between 1.1 and 1.3 years around $x = 310$ and between 2.2 to 2.5 years further offshore. Beyond 300 m, the amplitudes of the patterns are very small, possibly because at these depths the effects of mechanisms driving such patterns are also smaller. At transect 190, examination of Fig. 2(d) and Table 2 shows the yearly cycle is present throughout the transect, together with a cycle whose period varies between two and three years, and from 200 m to 490 m sometimes with a third cycle with period between one and two years. The periods of the SPOs are close to those found within monthly wave heights, monthly sea water levels and again, within NAO, as we will discuss in subsequent sections.

It is noteworthy that between 350 and 490 m offshore the dominant patterns have periods between 1 and 9.8 years at both transects, and that interannual patterns of variable periods were also found closer to the shore. This suggests that differences in the temporal patterns of the sandbar life cycle between different sides of the pier are not reflected in differences of the seabed elevation variations between those sides.

Finally, at some locations the detrending seems not to have worked properly. This is the case, for instance, between 370 and 390 m for transect 58, or at 140 and 200 m for transect 190. In all cases the patterns have periodicities close to 4 years and seem to have been misclassified within the trend or detrended signal. In some cases the uncertainty interval includes the window length size of 4 years even though the value of the peak lies incorrectly in the trend or detrended signal. In other cases it is the lack of a pattern of period above 4 years which leads to the identification of patterns between 3 to 4 years within the trend. Such issues are related to some limitations of SSA in identifying unequivocally patterns which have periodicities close to the size of the window length.

Patterns embedded within monthly mean wave heights (MWH), monthly mean water levels (MWL) and the monthly North Atlantic Oscillation (NAO) were also extracted following the same procedure and compared to those within the bathymetry to identify locations where similar patterns are observed. This will be discussed in more detail in Sect. 4.3. Linear correlations may also be computed; this was done throughout all the bathymetric surveys and the results are discussed next.

3.3. Spatial and spatio-temporal correlations between the bathymetry, waves, mean water level and NAO

The questions we want to address in this section are whether there are correlations between the bathymetry and the NAO, the MWL and the MWH and whether these phenomena have a local influence or act throughout the whole bathymetry. These phenomena are evaluated at a single location, as explained in Sec. 2, while there are measurements of the bathymetry at several locations along each transect used in our analyses. The correlations between the bathymetry and the NAO, the MWH and the MWL are computed using a simple correlation analysis. The correlations obtained at all bathymetric locations are shown in Fig. 5. The linear correlation analysis performed at all transects seems to corroborate the local correlations between embedded quasi-oscillations that were speculated about at transects 58 and 190 when comparing the LPOs and SPOs (shown in Table 2) to the atmospheric/hydrodynamic patterns deduced with SSA (see Sect.4.3). However, it is important to point out that a linear correlation analysis would permit neither to characterise the bedlevel patterns nor to suggest nonlinear correlations as was achieved with SSA.

The strength of the correlation is given by the correlation coefficient, r , shown in contour form in Figs 5. The maxima and minima of r show locations where the correlations are strongest, independently of the magnitude of r . In order to assess the overall strength of the (linear) correlation for each of the variables the following criteria may be useful: a) strong correlation when $0.5 < |r| \leq 1$; b) moderate correlation when $0.3 < |r| \leq 0.5$; c) weak correlation when $0.1 < |r| \leq 0.3$ and; d) no or very weak correlation when $0 < |r| \leq 0.1$. With these criteria, the percentage correlation between bedlevels and potential forcings may be computed for all the bathymetric profiles. If all the bathymetric surveys are considered, the overall strength of the linear correlations are as follows: 65.6% of the bathymetry is very weakly correlated and 34.4% is weakly correlated with NAO; 67.6% of the bathymetry is very weakly correlated and 32.4% is weakly correlated with MWH and; 28.3% of the bathymetry is very weakly correlated, 50.5% is weakly correlated and 21.2% is moderately correlated with MWL. Note the values of these correlation coefficients are very low, but they only give a measure of the linear correlation between the bathymetric evolution and the potential forcings, while SSA and MSSA give a nonlinear measure of correlations.

Table 3 shows for the first 4 EOFs from the MEOF analysis, the rows corresponding to each of the potential forcings, for transects 58 and 190 and then for the full set of bathymetric measurements at locations between and including these two transects. The potential forcings have been organised so that the one at the top has the largest (absolute value) contribution for EOF1, the second for EOF2, and so on. It is clear that each potential forcing may be unambiguously associated with a particular EOF. EOF4 has been included to show that for this eigenvector all potential forcings generally have a contribution at least an order of magnitude smaller than for eigenvectors EOF1 to EOF3. The eigenvector EOF1, corresponding to the largest eigenvalue, is correlated with NAO, regardless of whether we are considering transects 58 and 190, or all measured bathymetric profiles. Similarly, EOFs 2 and 3 are correlated with MWH and MWL respectively in both cases. Also, the magnitudes of the components corresponding to potential forcings in EOFs 1 to 3 are very close (in fact, they are equal for EOF1 and EOF2 at the level of accuracy considered here) whether we consider the two transects or all the bathymetric measurements together. Hence, the potential forcings are correlated in the same way with transects 58 and 190 as they are with the full set of measurements of the bathymetry and so we can use the latter

for subsequent analyses.

The MEOF analysis indicates that the first 3 EOFs are strongly linked to the three forcings considered and together they resolve 98.25% of the variance. Note how large the resolved variance is compared to the values of the correlation coefficients. This shows that even though the correlations are small, correlations with any other phenomenon would be significantly smaller and thus we can confidently say that NAO, MWH and MWL are the only relevant potential forcings. Also, since these three EOFs resolve so much of the variance, their associated PCs are used in the MSSA as input channels instead of the original dataset. This simplifies the MSSA considerably as the number of input channels is reduced from 1128 to 3.

The first 14 MSSA components of the filtered system – that is, the system consisting of the first 3 PCs as input channels, were analysed. Each of these components has its corresponding eigenvalue, spatiotemporal PC (ST-PC) and spatiotemporal EOF (ST-EOF). The criteria presented by Plaut and Vautard (1994) were used to identify coherent patterns within the ST-PCs. The method consists of finding pairs of consecutive eigenvalues which pass a number of tests; the pairs passing such tests correspond to a quasi-oscillatory pattern. The technique is described in more detail in the Appendix. It was found that all 7 pairs considered passed the test. No more pairs were analysed as these pairs resolve most of the variance.

Once pairs of eigenvalues corresponding to embedded quasi-oscillations are identified, the periods of these quasi-oscillations can be assessed. The first two pairs correspond to a yearly and a semi-yearly cycle (see Fig. 7; the time span is 120 months, or 10 years), and MSSA confirms that these cycles are correlated with the monthly wave heights as their amplitude is largest at channel 2, which corresponds to MWH. The other pairs have largest amplitude at channel 1, hence they are all correlated with the NAO. The first 4 of these pairs are linked to cycles of period of 3.92 mths, 3.14 mths, 8.62 mths and 2.96 mths. The last pair is associated with two cycles, of 5.4 mths and 2.98 mths. It is noteworthy that no collective interannual patterns seem to exist, even if such patterns have an important influence locally.

4. Discussion

4.1. Sensitivity to changes in window length for SSA

4.1.1. Transect 58:

At this transect a window length of 4 years chosen for the detrending analysis. However, the robustness of the results to small changes in window length was tested by varying the window between 3.3 and 6.6 years (so the window length span includes the sandbar life cycles observed north and south of the pier). It was found that the extrema had approximately the same values for all the window lengths considered, with some small deviations of their location along the transect depending on the window length considered. . The main difference observed occurred in the region of small variance, i.e. between 180 and 220 m offshore, where the trend signal did not capture any of the extrema when $M = 3.3$ years. However, window lengths between 4 to 6.6 years extracted trends that have similar characteristics.

The LPOs and SPOs within the two parts of the original signal thus obtained were then identified with SSA at a window length of 9 years and a window length of 8.12 years. Again, the dominant patterns were found to be robust to changes in window length, but the window length of 9 years captured some of the fluctuations better.

4.1.2. Transect 190:

Since the window length of 4 years was best at transect 58 detrending was performed initially at this window length. The trends shown in Fig. 1 are at this window length for most of the transect except between 130 and 170 m offshore. In this region the 4 year window did not resolve the travelling patterns adequately, so it was necessary to experiment with slight changes to window length to obtain a coherent picture. The amount of variance resolved by the patterns, however, is the same as that with a window of 4 yrs, and the characteristics of the travelling patterns are therefore robust (because these slight changes do not introduce more information). It seems that the sensitivity in window length in this region is due to the change in type of behaviour between the region closer to the shore and the patterns travelling seawards between 140 and 270 m (see the patterns developing from year 15 onwards in Plot b,ii) of Fig. 1, for instance).

4.2. Comparison with previous Duck studies

Our results compare well with the wavelet analyses presented by Reeve et al. (2007), which focused on temporal scales of variability at Tr. 62. We

shall use our results at Tr. 58 for the comparison, since Tr. 62 lies only around 100 m south of Tr. 58 and hence sufficiently nearby for variations in underlying oscillations to be small.

Reeve et al. (2007) found that between 100 and 190 m offshore most of the variance corresponded to periodicities between 8 and 12.8 months. This agrees well with the yearly pattern found at Transect 58; however, our trend analysis has highlighted that LPOs are also present in this region, with periodicities varying between 3 and 12 years depending on the location. SSA at 260 m led to three dominant quasi-oscillations of periods 4.5-5.9 years, 1.6-2 years and 3.6-4.8 years. This agrees relatively well with Reeve et al. (2007) who found that at $x = 260$ m, 25.95% of the variance corresponded to periodicities between 1.3 and 1.8 years, which would be linked to the 1.6-2 yearly patterns identified at Transect 58. It is noteworthy that at $x = 410$ m the pattern with a period of 6 – 8 years identified by Reeve et al. (2007) was not observed. Therefore, the alongshore homogeneity assumption breaks to some degree at this position. This does not significantly affect the analysis presented here since it is not based on this assumption.

The large variability of temporal scales identified within the dynamics is a consequence of the extremely non-stationary behaviour of beach profiles at Duck. Nonstationarity of the patterns, observed by Reeve et al., is also evident with SSA and had been noted by Li et al. (2005) in an earlier wavelet study at Duck. Yiou et. al. (2000) have pointed out that SSA and wavelets can both identify nonstationary behaviour in time series, contrary to more standard time series analysis methods. Also, although wavelets have been the method of choice for intermittent time series analysis, a multi-scale SSA may be produced using a moving window length and the eigenvectors of the resulting lag-correlation matrix are equivalent to data-adaptive wavelets. While wavelet analysis may appear conceptually simple, it is not without difficulties. For instance, the Heisenberg uncertainty principle implies that the optimizing wavelet needs to satisfy a trade-off between localisation in time and in frequency (Yiou et. al., 2000; Grinsted et al., 2004). It would be interesting to analyse correlations between the bed level behaviour with cross-wavelets between the bed level variations and the suggested potential forcings, at individual locations, in particular because this would permit the identification of the relative phases between the two time series, which is not straightforward with SSA. This would provide an additional measure of the correlation between the bedlevels and the phenomena time series at given locations.

Sequential beach changes performed by Birkemeier (1984) and Lippmann et al. (1993) can be compared to the results presented here. Birkemeier's study covered the period between 1981 and July 1984, i.e from $t = 0$ to $t = 3$ yrs, while Lippmann et al.'s study took place between October 1986 and September 1991, i.e. from $t = 5.35$ to 10.17 yrs. In both studies the shoreline moved on and offshore, always lying between $x = 100$ m and $x = 140$ m. This agrees well with the first spatial region identified with SSA at both window lengths, which implies that these quasi-oscillatory patterns are linked to those of the shoreline.

There is also good agreement between Birkemeier and Lippmann et al.'s studies and this one in relation to the region identified as most dynamic. In this study it is found, for instance, that between 130 m and 350 m several quasi-periodic cycles may dominate the dynamics (see Plots (a,ii) and (a,iii) as well as Plots (b,ii) and (b,iii) in Fig. 1); Birkemeier and Lippmann et al. also found that this was the most dynamic region in terms of number of bars and in terms of bar motion. In their study, the inner bars moved on and offshore between 130 m and 330 m, and the outer bars generally between 200 and 450 m. Moreover, Lippmann et al. (1993) showed that the inner bar oscillates seasonally around a fixed position of around 200 m, while Birkemeier (1984, as cited by Lippmann et al. (1993)) showed that at transects 62 and 188 the inner bars had significant intra-annual variations and remained generally shorewards of 200-210 m offshore. In this study it is also found that several intra-annual patterns exist shorewards of 200-210 m, as shown in Plots (a,iii) and (b,iii) of Fig. 1.

4.3. Underlying quasi-periodic patterns in potential forcing mechanisms based on SSA and possible correlations with bathymetric patterns

It is expected that a yearly cycle will be embedded within the wave data and hence may potentially be correlated to the bathymetric yearly cycle. To investigate this, we used the wave data from a wave gauge array, consisting of 15 pressure gauges mounted 0.5 m off the sea floor, at a depth of around 8 meters. The array is located between 835 to 955 m offshore and between 735 and 990 m alongshore, i.e. in the vicinity of transect 58. A rose plot of wave directions (not shown) indicates that the wave crests at this position are almost parallel to the shore, as all the monthly averaged wave directions are between 54° and 108° North, with 68.5% of them in the 73° - 90° range. Moreover, at this location the mean wave period is around 9 s, with a standard deviation of 0.76 s; thus, there is little variation in the monthly averaged

wave period, T_p . Therefore, the only wave parameter showing significant variation at this location is the wave height. Since the bathymetric analysis is performed on monthly interpolations of the data and our interest lies in the long-term (yearly to decadal) evolution of the seabed, we deem it sufficient to consider the monthly averaged wave heights at this location. This is equivalent to utilising appropriate means in the wave forcings in relation to the timescales of the studied bathymetric change (Cayocca, 2001).

SSA of the monthly averaged wave heights clearly indicate the two main underlying quasi-oscillations are predominantly annual and semi-annual, respectively; these two oscillations are shown in Fig. 4. We hypothesise, therefore, that the semi-annual and the annual cycles found in the bathymetric profiles are very likely to be induced by the monthly-averaged wave climate. This is corroborated by the MEOF and the MSSA studies discussed in Sect. 4.4 and confirms extensive work by previous authors (Lippmann et al., 1993; Plant et al., 1999; Larson and Kraus, 1994; Horrillo-Caraballo and Reeve, 2008, and references therein), who have identified the wave climate as one of the dominant forcing mechanisms of nearshore dynamics.

As mentioned in the introduction, storm surges have been shown to have an important influence on coastal erosion. Although the variation of water depth throughout the bathymetry is unknown, a measure of the local water depth, or the mean water level, MWL, is given by tidal gauge measurements at the site, collected by NOAA. An SSA of the MWL highlights two inter-annual oscillations below 9 years, with periods of 5.7-6.2 yrs and 1.89-2 yrs. Four intra-annual patterns are identified too, with periods of 2.47-2.53 mths, 3.9-4.1 mths, 5.8-6.1 mths and one year. Some of these patterns are similar to those embedded within the bathymetry at some locations. Note that Kirby and Kirby (2008) identify neap-spring tide cycles and seasonal cycles within tidal mudflats to be linked predominantly to tides and wave conditions, with the bathymetric long-term patterns being strongly linked to NAO. Considering the interannual MWL patterns we identified at Duck, MWL may be influencing such long-term patterns in the bathymetry, and not just tidal or seasonal patterns. However, Kirby and Kirby's study as well as other investigations on the influence of climatic patterns on bedlevel variations would suggest NAO may be influencing bedlevel variations at Duck (Ranasinghe et al., 2004; Kirby and Kirby, 2008; Różyński, 2010).

To check which patterns are embedded within the NAO time series, NAO data was obtained from the coastal research unit of the University of East Anglia (see <http://www.cru.uea.ac.uk/~timo/datapages/naoi.htm>) and analysed

with SSA. The annual NAO index between 1850 and 1999 was extracted from the dataset and SSA was applied using a window length of 40 and 50 years - this allows the identification of interannual as well as some decadal patterns of oscillation underlying the dynamics. The interannual patterns identified are cycles of 7.1 to 8.8 years and 2.7 to 2.9 years, with a smaller contribution from cycles of periodicity between 3.8 to 5 years; another contribution with periodicity between 12 and 13 years is also found. These periodicity values are robust to window length changes both in the SSA and the correlogram SDA tests. Some of the periodicities within the bed level data coincide with the observed processes but not others. One should not be seeking a physical explanation for all the statistics, as noise produced by, for instance, transverse bars or bar splitting, may cause some variations in the observations (Kirby and Kirby, 2008). However, conceptual models describing the sediment transport and hydrodynamic processes expected to result in the observed patterns need to be based on links between the patterns so that causalities can be identified. For instance, Różyński (2010) found that at Lubiatowo there was a weak correlation between NAO and the wave climate. Ranasinghe et al. (2004), on the other hand, found that accretion patterns in the Southern end of Narrabeen Beach (New South Wales, Australia) could be attributed to negative SOI index phases linked to a reduced number of tropical cyclones and East Coast lows in the Australian East Coast which pushed the storms further south leading to a reduction of their effects on the side of pocket beaches sheltered by headlands. In the North Atlantic, the NAO has been shown to produce variations in sea level over decadal timescales (Gehrels and Long, 2007). At short to medium timescales NAO index phases are likely to be linked to changes in sea level pressure lows and highs and have an effect on the direction and intensity of the storms, in analogy with the observed effects of the SOI in the South Pacific Ocean. Most research so far has identified links between climatic indexes and erosion and accretion patterns, but it is more difficult to assess their effects on the dynamics of NOM systems. Also, at Duck the pier may be introducing patterns similar to those observed on sheltered beaches depending on the direction of the incoming waves. Additional research looking at NAO index phases would be necessary to propose any conceptual model on how NAO may be influencing the dynamics at Duck. This is beyond the scope of the current investigation which only concerns quantification of cyclic patterns and is left for future studies. In order to analyse further whether the potential forcings discussed in this section are correlated with seabed level measurements

throughout the bathymetry, and which collective patterns of behaviour they may be correlated with, we performed spatio-temporal correlation analyses using MEOF and MSSA and these will be discussed next.

4.4. Spatial and spatiotemporal correlations between potential forcings and bathymetry and possible causalities

As shown in Sect. 3.3, the MEOF has permitted the isolation of the effects of the different potential forcings on the bathymetry because each potential forcing is most strongly correlated with one of the first 3 EOFs: the NAO with EOF1, the monthly wave heights (MWH) with EOF2 and the monthly mean water level (MWL) with EOF3.

Figs. 5 permit the identification of regions where each of the potential forcings is more strongly correlated with seabed evolution, simply by locating the regions where the correlations are highly positive or highly negative. Note that the region where the analysis was performed extends from 80 to 520 m offshore, rather than between 100 and 490 m, as was the case in the previous sections. As explained before, this was done to capture the behaviour around the shoreline and the behaviour offshore more fully.

Since the first EOF captures the largest proportion of the variance and it is linked to the NAO, it appears that the NAO is more strongly correlated with the seabed than are the waves at the time and space scales under consideration. Plot 5(a) shows the distribution of correlations between the seabed and NAO, and highlights the complex interactions between them; the regions of positive and negative correlation are clearly visible in the plot. It shows the correlations are either very weak (with $|r| < 0.1$) or weak (with $0.1 < |r| \leq 0.3$). Weak correlations occur 1) North of the pier between 600 m and 1100 m alongshore and 80 to 100 m cross-shore; 2) South of the pier between -100 m and 100 m alongshore and 360 m and 490 m cross-shore and; 3) all along the shore between approximately 150 m and 240 m cross-shore. However, even though the correlation is low, it is found that the correlation coefficient contours give valuable information and the locations of extrema (either positive or negative) are more important than the magnitude of the extrema. An analysis of extrema close to the pier shows, for instance, that there are stronger correlations between NAO and the seabed between 180 and 290 and between 350 and 450 m offshore than at other cross-shore locations. Moving northward from the pier these regions, while remaining distinct, move closer to the shore. Thus, at transect 58, the largest negative correlations occur now between 150 and 200 and between 320 and 380 m

offshore (approximately), with two regions of positive correlations appearing between 250 and 280 m and seawards of 450 m. Southwards of the pier, the region of negative correlation is around 150 and 230 and a region of positive correlations appears between 350 and 450 m. Note that although the magnitude of the correlations is low the variance resolved by the EOF associated with the NAO is large (see Table 3) (remember that the correlation coefficient is linked to the spatial EOFs of the MEOF covariance matrix). The variance is a relative measure indicating that along this direction the correlations with other phenomena will be much weaker.

The regions where NAO and the bathymetry are more likely to be correlated (or anti-correlated) relative to other seabed locations - even if in absolute terms the correlations are everywhere weak - and the correlations between them deduced from the SSA at transects 58 and 190 seem to be consistent with one another. For instance, Table 2 shows that, for transect 58, regions seawards of 150 m have one underlying cycle at a periodicity found within the NAO signal: as we know, the NAO has 3 interannual underlying cycles with periods of around, 2, 5 and 6-8 years, respectively, and if for instance we choose the 250m offshore location, we see that the period of 5yrs is contained within the bathymetric pattern with period 5.4 ± 0.9 ; at 480 m and 490 m two of the dominant bathymetric cycles identified have periods that are close to two dominant patterns within NAO, namely the 2 and the 6-8 yearly cycles. For transect 190, patterns of the same periodicity as those of the NAO were found both from 120 to 200 m and beyond 450 m offshore. A possible physical mechanism for the NAO to influence the bathymetry is indirectly through the thin layer of water in the nearshore, producing cyclic patterns of behaviour in the bathymetry with periodicities close to its own underlying cyclic patterns.

The MWH is the dominant potential forcing in EOF2 and the distribution of correlations between MWH and the seabed is shown in plot 5(b). Again, the regions around positive and negative correlation extrema indicate regions where the MWH is more likely to be correlated with the seabed oscillations. There is agreement between the regions identified here and those where the waves may have an important effect: for instance, in the swash zone, i.e. between 80 and 90 m offshore, where there are positive correlations. Looking at the SSA results in more detail, we know from the SSA that the wave height has a yearly pattern and that such a pattern is also present shorewards of 310 m at transect 58, and all along the transect at transect 190. As discussed above, the correlation contour plot 5(b) seems to indicate, indeed, that the

correlation between the seabed and the waves near the pier and close to the shoreline is stronger than at other bathymetric locations, as evidenced by the region of negative correlations occurring between 130 and 250m offshore and between 0 and 800 m alongshore, approximately. As we approach transect 190, there appears to be a correlation minimum between 200 and 260 and a correlation maximum between 380 and 500 approximately, even though the correlations are overall weak. On the other hand, at transect 58 there seem to be more variations in the correlation values, which may indicate there is more variability in the interaction between the waves and the seafloor along this transect than along transect 190.

Finally, plot 5(c) shows the distribution of correlations between the seabed and the MWL. Plot 5(c) show there are regions of moderate correlation and the distribution of correlation coefficients is symmetric around the pier. The plots suggest the greatest correlation with the mean water level could be within 120-200 m and 380-500 m along transects 58 and 190. This is relatively consistent with the locations where a 1.4-2.2 yearly cycle was found (see Table 2) and, thus, with the wavelet findings of Reeve et al. (2008). This work not only confirms the presence of those bathymetric patterns but also suggests the physical mechanism influencing them is one which, at least partially, contributes to changes in water level variations. These could be any of the storm surge components.

The rest of this section focuses on the MSSA results. As presented in Sect. 3.3, no interannual coherent, spatio-temporal patterns are found when all the bathymetric measurements and the three potential forcings are analysed together, even when locally these patterns are clearly identified. This is an important difference with the SSA/MEOF analyses, where the local bathymetric patterns could be attributed to any of the three forcings considered, depending on the characteristics of the patterns and the region under consideration. However, the absence of coherent interannual, spatiotemporal patterns possibly means that the mechanism forcing such behaviour acts locally and not globally at these temporal scales.

For studies including monthly responses, the results in Sect. 3.3 show that the two most important collective patterns, the yearly and the semi-yearly cycle, are both correlated with the monthly wave heights. This agrees well with the SSA results summarized in Table 2, showing the ubiquitous presence of the annual cycle all along Transects 58 and 190. Finally, except for the semi-annual pattern all the intraannual collective patterns identified are correlated with the NAO.

5. Summary and Conclusions

In summary, local and collective bathymetric quasi-periodic patterns of oscillation were identified from monthly profile surveys spanning 26 years, from July 1981 to January 2006, at the USACE field research facility in Duck, North Carolina. The local analyses were based mostly on the outmost transects of the surveyed domain, but the collective patterns were computed using all surveyed bathymetric profiles, including those in the vicinity of the pier. Correlations with three potential forcings, namely the monthly wave heights (MWH), monthly mean water levels (MWL) - which include the storm surges as well as the tide - and the large scale atmospheric index the North Atlantic Oscillation (NAO), were discussed.

The local seabed patterns and their spatial correlations with NAO, MWH and MWL were first analysed using SSA, which showed the highly nonstationary behaviour of the bedlevels along transects 58 and 190. It was shown 1) that a quasi-yearly cycle was embedded at most bathymetric locations and this is likely to be correlated with the quasi-yearly pattern within the monthly averaged wave climate; 2) the local behaviour is highly nonstationary as observed by previous studies; 3) patterns with periodicities in the range between 1.4 and 2.2 were found at some seabed locations and also within the MWL, providing an explanation for the potential origin of such patterns and 4) several interannual patterns were identified, some of which are likely to be correlated with the NAO. Some statistics may be attributed to noise. As in other studies on Duck, differences in the behaviour North and South of the pier were observed.

Linear correlation coefficient contours were computed throughout all bathymetric surveys. The regions at the North and South boundaries of the domain where the magnitude of the correlation coefficient was largest (relative to other locations along the transect) seem to agree broadly with those identified with SSA, even though the correlation coefficient gives a measure of linear correlation while SSA is a nonlinear measure; in fact linear correlation analysis cannot characterise the nonlinear quasi-oscillations. It was found that linear correlations with the NAO and the MWH were weak to very weak. For the MWL, the correlation contours were symmetric North and South of the pier and there was a region between 100 and 200 metres offshore of moderate correlation between bedlevels and MWL for all the surveys.

The last component of the analysis consisted of the identification of spatio-temporal oscillations and their nonlinear correlation with NAO, MWH

and MWL. This indicated that there are no patterns that are coherent throughout the bathymetry at yearly timescales, but there are a few at monthly scales which are correlated with the NAO. This is consistent with the highly localised nature of the interannual quasi-oscillatory patterns that was observed with SSA. This study is a preliminary step towards, for instance, an understanding of the potential effects of increased storminess (due to climate change) on bathymetric evolution, or attempts to model nearshore long-term morphodynamics.

6. Acknowledgements

This work was supported by an RCUK Academic Fellowship from the EPSRC (Grant number EP/C508750/1) and a Research and Innovation Fellowship award from the University of Plymouth, UK. Thanks to Tom Lippmann and David Huntley for useful discussions. The editors and two anonymous referees are thanked for valuable comments.

References

- Akima, H., Oct 1970. A new method of interpolation and smooth curve fitting based on local procedures. *Journal of the ACM* 17 (4), 589–602.
- Allen, M. R., Robertson, A. W., 1996. Distinguishing modulated oscillations from coloured noise in multivariate datasets. *Clim. Dyn.* 12 (11), 775–784.
- Birkemeier, W. A., 1984. Time scales of nearshore profile changes. In: *Proceeding of the 19th Conference on Coastal Engineering*. New York (ASCE), pp. 1507–1521.
- Blackman, R. B., Tukey, J. W., 1958. *The measurement of power spectra from the point of view of communication engineering*. Dover, New York.
- Bowen, A. J., 1980. Simple models of nearshore sedimentation: beach profiles and longshore bars. In: McCann, S. B. (Ed.), *The Coastline of Canada*. Geological Survey of Canada, Ottawa, pp. 1–11.
- Bowen, A. J., Guza, R. T., 1978. Edge waves and surf beat. *J. Geophys. Res.* 83, 1913–1920.

- Bowen, A. J., Inman, D. L., 1971. Edge waves and crescentic bars. *J. Geophys. Res.* 76.
- Broomhead, D. S., King, G. P., 1986. Extracting qualitative dynamics from experimental data. *Physica D* 20, 217–236.
- Cayocca, F., 2001. Long-term morphological modeling of a tidal inlet: the Arcachon basin, France. *Coast. Eng.* 42, 115–142.
- Coco, G., O’Hare, T. J., Huntley, D. A., 1999. Beachcusps: A comparison data and theories for their formation. *J. of Coastal Res.* 15, 741–749.
- Dodd, N., Blondeaux, P., Calvete, D., de Swart, H. E., Falqués, A., Hulscher, S., Różyński, G., Vittori, G., 2003. Understanding coastal morphodynamics using stability methods. *Jour. Coast. Res.* 19 (4), 849–865.
- Evans, R. L., November 2004. Rising sea levels and moving shorelines. *Oceanus* WHOI Magazine.
- Falques, A., Coco, G., Huntley, D. A., 2000. A mechanism for the generation of wave-driven rhythmic patterns in the surf zone. *Jour. Geophys. Res. - Oceans* 105, 24071–24087.
- Gallagher, E. L., Elgar, S., Guza, R. T., 1998. Observations of sand bar evolution on a natural beach. *Jour. Geophys. Res.* 103 (C2), 3203–3215.
- Garnier, R., Calvete, D., Falques, A., Caballeria, M., 2006. Generation and nonlinear evolution of shore-oblique/transverse sand bars. *J. Fluid Mech.* 567, 327–360.
- Gehrels, W. R., Long, A. J., 2007. Sea level is not level: the case for a new approach to predicting UK sea-level rise. *Geography* 93 (1), 11–16.
- Ghil, M., Allen, M. R., Dettinger, M. D., Ide, K., Kondrashov, D., Mann, M. E., Robertson, A. W., Saunders, A., Tian, Y., Varadi, F., Yiou, P., 2002. Advanced spectral methods for climatic time series. *Rev. Geophys.* 40 (1), 1–1–1–41.
- Ghil, M., Mo, K. C., 1991. Intraseasonal oscillations in the global atmosphere. part I: Northern Hemisphere and tropics. *J. Atmos. Sci.* 48, 752–779.

- Gilmore, R., Lefranc, M., 2002. The topology of Chaos; Alice in Stretch and Squeezeland, First Edition, John Wiley and Sons, Inc, New York, 518 pp.
- Grassberger, P., 1986. Do climate attractors exist? *Nature* 323, 609–612.
- Grassberger, P., Procaccia, I., 1983. Measuring the strangeness of strange attractors. *Phys. D* 9, 189–208.
- Grinsted, A., Moore, J. C., Jevrejeva, S., 2004. Application of the cross wavelet transform and wavelet coherence to geophysical time series. *Nonlin. Proc. Geophys.* 11, 561–566
- Holman, R. A., Bowen, A. J., 1982. Bars, bumps, and holes: Models for the generation of complex beach topography. *J. Geophys. Res.* 87 (C1), 457–468.
- Holman, R. A., Lippmann, T. C., 1987. Remote sensing of nearshore bar systems – making morphology visible. *Proceedings of Coastal Sediments '87 ASCE*, 927–944
- Holman, R. A., Sallenger, A. H., 1986. High energy nearshore processes. *EoS Trans. AGU* 67, 1369–1371.
- Horrillo-Caraballo, J. M., Reeve, D. E., 2008. An investigation of the link between beach morphology and wave climate at Duck, N.C., USA. *Jour. Flood Risk Management* 1 (2), 110–122.
- Howd, P. A., Birkemeier, W. A., 1987. Beach and nearshore survey data: 1981-1984. CERC Field Research Facility. Tech. rep., U. S. Army Eng. Waterways Expt. Stn., Coast. Eng. Res. Ctr., Vicksburg, MS.
- Kirby, J. R., Kirby, R., 2008. Medium timescale stability of tidal mudflats in Bridgwater Bay, Bristol Channel, UK: Influence of tides, waves and climate. *Cont. Shelf Res.* 28, 2615–2629
- Klein, M. D., Schuttelaars, H. M., 2006. Morphodynamic evolution of double-barred beaches. *J. Geophys. Res.* 111 (C06017).
- Komar, P. D., 1971. Nearshore circulation and the formation of giant cusps. *Geol. Soc. Am. Bull.* 82, 2643–2650.

- Kuriyama, Y., Ito, Y., Yanagishima, S., 2008. Medium-term variations of bar properties and their linkages with environmental factors at Hasaki, Japan. *Mar. Geol.* 248 (1-2), 1–126.
- Larson, M., Kraus, N. C., 1994. Temporal and spatial scales of beach profile change, duck, north carolina. *Mar. Geo.* 117, 75–94.
- Lee, G., Nicholls, R. J., Birkemeier, W. A., 1998. Storm-driven variability of the beach-nearshore profile at duck, north carolina, usa, 1981-1991. *Mar. Geol.* 148, 163–177.
- Lee, G. H., Birkemeier, W. A., 1993. Beach and nearshore survey data: 1985-1991. CERC Field Research Facility. Tech. rep., Defense Technical Information Center OAI-PMH Repository [<http://stinet.dtic.mil/oai/oai>] (United States).
URL <http://handle.dtic.mil/100.2/ADA266371>
- Li, Y., Lark, M., Reeve, D., 2005. Multi-scale variability of beach profiles at Duck: A wavelet analysis. *Coast. Eng.* 52 (12), 1133–1153.
- Lippmann, T. C., Holman, R. A., 1990. The spatial and temporal variability of sand bar morphology. *Jour. Geophys. Res.* 95 (C5), 11575–11590.
- Lippmann, T. C., Holman, R. A., Hathaway, K. K., 1993. Episodic, nonstationary behavior of a double bar system at Duck, North Carolina, U. S. A. *Jour. Coastal Res.* 15, 49–75.
- Miller, J. K., Dean, R. G., 2006. Shoreline variability via empirical orthogonal function analysis: Part I. Temporal and spatial characteristics. *Coast. Eng.* 54 (2), 111–131.
- Moron, V., Vautard, R., Ghil, M., 1998. Trends, interdecadal and interannual oscillations in global sea-surface temperatures. *Climate Dynamics* 14, 545–569.
- Mote, P. W., Clarke, H. L., Dunkerton, T. J., Harwood, R. S., Pumphrey, H. C., 2000. Intraseasonal variations of water vapor in the tropical upper troposphere and tropopause region. *Jour. Geophys. Res.* 105 (D13), 17457–17470.

- Nicholls, R. J., Birkemeier, W. A., Lee, G., 1998. Evaluation of depth of closure using data from Duck, NC, USA. *Mar. Geo.* 148, 179–201.
- Niedoroda, A. W., Tanner, W. F., 1970. Preliminary study on transverse bars. *Mar. Geol.* 9, 41–62.
- North, G. R., Bell, T. L., Cahalan, R. F., Moeng, F. J., 1982. Sampling errors in the estimation of empirical orthogonal functions. *Mon. Wea. Rev.* 110, 699–706.
- Papadopoulos, A., Tsimplis, M. N., 2006. Coherent coastal sea-level variability at interdecadal and interannual scales from tide gauges. *J. Coast. Res.* 22 (3), 625–639.
- Pape, L., Ruessink, B. G., 2008. Multivariate analysis of nonlinearity in sandbar behavior. *Nonlinear Processes in Geophysics* 15 (1), 145–158.
URL <http://www.nonlin-processes-geophys.net/15/145/2008/>
- Plant, N. G., Holman, R. A., Freilich, M. H., Birkemeier, W. A., July 1999. A simple model of interannual sandbar behaviour. *Jour. Geophys. Res.* 104, 15755–15776.
- Plaut, G., Vautard, R., 1994. Spells of low-frequency oscillations and weather regimes in the Northern Hemisphere. *J. Atmos. Sci* 51 (2), 210–236.
- Pruszek, Z., Różyński, G., Szmytkiewicz, M., Skaja, M., 1999. Quasi-seasonal morphological shore evolution response to variable wave climate. In: *Coastal Sediments Conference Proceedings, ASCE*. pp. 1081–1093.
- Ranasinghe, R., McLoughlin, R., Short, A., Symonds, G., 2004. The Southern Oscillation Index, wave climate and beach rotation. *Mar. Geol.* 204, 273–287.
- Rattan, S. S. P., Ruessink, B. G., Hsieh, W. W., 2005. Non-linear complex principal component analysis of nearshore bathymetry. *Nonlin. Processes Geophys.* 12 (5), 661–670.
- Reeve, D., Li, Y., Lark, M., Simmonds, D., May 2007. An investigation of the multi-scale temporal variability of beach profiles at Duck using wavelet packet transforms. *Coast. Eng.* 54 (5), 401–415.

- Reeve, D. E., Horrillo-Caraballo, J. M., Magar, V., 2008. Statistical analysis and forecasts of long-term sandbank evolution at Great Yarmouth, UK. *Estuar. Coast. Shelf Sci.* 79 (3), 387–399.
- Robertson, A. W., 1996. Interdecadal variability over the north pacific in a multi-century climate simulation. *Clim. Dyn.* 12, 227–241, in the appendix there is a very clear explanation of the MSSA and the Monte Carlo tests to separate signal from noise and identify modulated oscillations from a multivariate timeseries.
- Różyński, G., Larson, M., Pruszek, Z., 2001. Forced and self-organised shoreline response for a beach in the southern Baltic Sea determined through Singular Spectrum Analysis. *Coast. Eng.* 43, 41–58.
- Różyński, G., 2003. Data-driven modeling of multiple longshore bars and their interactions. *Coast. Eng.* 48, 151–170.
- Różyński, G., 2005. Long-term shoreline response to a nontidal, barred coast. *Coast. Eng.* 52, 79–91.
- Różyński, G., 2010. Long-term evolution of Baltic Sea wave climate near a coastal segment in Poland; its drivers and impacts. *Ocean Eng.* 37, 186–199.
- Ruelle, D., 1990. Deterministic chaos: The science and the fiction. *Proc. Royal Soc. London A* 427, 241–248.
- Ruessink, B. G., Kroon, A., 1994. The behaviour of a multiple bar system in the nearshore zone of Terschelling: 1965–1993. *Mar. Geol.* 121, 187–197.
- Ruelle, D., 1990. Deterministic chaos: The science and the fiction. *Proc. Royal Soc. London A* 427, 241–248.
- Ruessink, B. G., Wijnberg, K. M., Holman, R. A., Kuriyama, Y., Van Enckevort, I. M. J., 2003. Intersite comparison of interannual nearshore bar behavior. *J. Geophys. Res.* 108 (C8), 3249.
- Shand, R. D., Bailey, D. G., 1999. A review of net offshore bar migration with photographic illustrations from Wanganui, New Zealand. *J. Coastal Res.* 15, 365–378.

- Shand, R. D., Bailey, D. G., Shepherd, M. J., 1999. An inter-site comparison of net offshore bar migration characteristics and environmental conditions. *J. Coastal Res.* 15, 750–765.
- Shand, R. D., 2007. Bar splitting: system attributes and sediment budget implications for a net offshore migrating bar system. *J. Coastal Res.* SI 50 (Proceedings of the 9th International Coastal Symposium, Gold Coast, Australia), 721–730.
- Southgate, H. N., Möller, I., 2000. Fractal properties of coastal profile evolution at Duck, North Carolina. *J. Geophys. Res.* 105 (C5), 11489–11507.
- Southgate, H. N., Wijnberg, K. M., L., Capobianco, M., Jansen, H., 2003. Analysis of field data of coastal morphological evolution over yearly and decadal timescales. part 2: Non-linear techniques. *Jour. Coast. Res.* 19, 776–789.
- Vautard, R., Ghil, M., 1989. Singular spectrum analysis in nonlinear dynamics, with applications to paleoclimatic time series. *Physica D* 35, 395–424.
- Welch, P. D., June 1967. The use of fast fourier transform for the estimation of power spectra: a method based on time averaging over short, modified periodograms. *IEEE Trans. Audio Electroacoustics* 15 (2), 70–73.
- Wijnberg, K. M., Kroon, A., 2002. Barred beaches. *Geomorphology* 48, 103–120.
- Wijnberg, K. M., Terwindt, J. H. J., 1995. Extracting decadal morphological behaviour from high-resolution, long-term bathymetric surveys along the Holland coast using eigenfunction analysis. *Mar. Geol.* 126, 301–330.
- Winant, C. D., Inman, D. L., Nordstrom, C. E., 1975. Description of seasonal beach changes using empirical eigenfunctions. *Jour. Geophys. Res.* 80, 1979–1986.
- Wright, L. D., Short, A. D., 1984. Morphodynamic variability of surf zones and beaches: a synthesis. *Mar. Geol.* 56 (C7), 11575–11590.
- Yiou, P., Sornette, D., Ghil, M., 2000. Data-adaptive wavelets and multi-scale singular-spectrum analysis. *Physica D* 142, 254–290.

A. Description of methods

A.1. SSA and SDA

The fundamental theory of SSA has been discussed by Broomhead and King (1986), Vautard and Ghil (1989) and Ghil et al. (2002) in relation to discrete time series analysis. The following summarises the SSA methodology. Suppose the bed level variable $z(t)$, sampled at times $t = i\tau_s$, $i = 1, 2, \dots, N$ (N being the length of the time series and τ_s the sampling interval), at a given cross-shore and long-shore location (x, y) , characterises the seafloor dynamical system. First, the noise part of the bed level time series may be identified by computing the statistical dimension, S , which is found by constructing a secondary, M -dimensional sequence, $Z_n = (z_n, z_{n+1}, \dots, z_{n+M-1})$, for $n = 1, 2, \dots, N - M + 1$, where $M < N$ is the window length and $z_n = z(n\tau_s)$. Time scales of the dynamics that can be reconstructed from this time series are between τ_s and $\tau_w = M\tau_s$, where τ_w is the window time span. Then, the eigenvalue problem

$$\mathbf{C}\mathbf{e}^{(k)} = \lambda_k \mathbf{e}^{(k)}, \quad (1)$$

must be solved, where \mathbf{C} is the covariance matrix of the sequence Z_n and λ_k are the eigenvalues associated with the eigenvector $\mathbf{e}^{(k)}$. The square roots of λ_k are called the singular values, with their set being called the *singular spectrum*. The largest singular values relate to the directions that resolve most of the variance, with the rest being a representation of the noise component and appearing as an approximately flat floor in a plot of singular value *vs.* singular value rank (with the singular values ordered from largest to smallest). The dimension S , then, will be given by the number of singular values above this floor.

Now, each singular value λ_k has an associated principal component (PC), defined as

$$A_k(i\tau_s) = \sum_{j=1}^M z(\{i + j - 1\}\tau_s) e_j^{(k)}. \quad (2)$$

Once the PCs have been identified, the part of the original time series related to that PC, or to a combination of K PCs, may be obtained by computing

$$RC(i\tau_s) = \frac{1}{M_i} \sum_{k \in K} \sum_{j=L_i}^{U_i} A_k(\{i - j + 1\}\tau_s) e_j^{(k)}, \quad (3)$$

where RC, the *reconstructed component*, is the part of the original signal related to the PC combination. The values of the renormalisation factor,

M_i , and the lower and upper bound, L_i and U_i , respectively, depend on the time at which the reconstruction is being evaluated.

The frequencies that can be resolved with SSA depend on the choice of window length, M , which is a free parameter of the method. However, the patterns extracted should be robust to small changes in window length. Here the depth time series were divided into a trend and a detrended signal. The trend generally contains a part found by linear regression of the data, as well as the RC corresponding to the first few eigenvectors of the SSA at a given window length M . These first few eigenvectors generally contain all oscillations within the original time series that have periods above M , which in this case was taken as four years. From the trend thus computed, long-period oscillations (LPOs) were extracted, while from the detrended signal short-period oscillations (SPOs) may be characterised. Cycles of three to five years may fall in either signal because of the window length selected for the detrending analysis (this will be discussed in more detail in subsequent sections).

In natural systems, there is the additional problem of red noise (which is noise composed of many random frequencies but, in contrast to white noise where all frequencies have equal intensity, the intensity of the lower frequencies is stronger) that can be removed from the data by using either Monte Carlo or chi-squared tests. In this work a chi-squared test was applied on 100 red-noise surrogates; these surrogates were projected onto the SSA eigenvector basis, and the distribution of projections was approximated as chi-squared with $3M/N$ degrees of freedom. Then those projections that fell outside a percentile range of 2.5% to 97.5% were identified as being part of the signal, and could thus be dissociated from the red noise in the time series.

Spectral density analysis (SDA) is a well established technique to analyse oscillatory patterns in time series. The spectral density was computed using Welch's (Welch, 1967) periodogram method and the Blackman-Tukey correlogram approach (Blackman and Tukey, 1958). The former consists of dividing the input signal into short segments and computing a modified periodogram for each segment, thus leading to a set of periodograms which are finally averaged to obtain an estimate of the spectral density function. In the latter a windowed Fast Fourier Transform of the autocorrelation function is equated to the spectral density.

It is well known that the spectral density is a measure of the energy contained in the system. By analysing the spectral density it is possible to characterise how the total energy is distributed and, in particular, to find the

frequencies that contribute the most to it.

A.2. MEOF/Correlation analysis

Multivariate empirical orthogonal functions can be used to study the relationship between different physical variables that are sampled at the same set of times. It can be thought of as a prefiltering step for MSSA/MEEOF analysis: instead of performing the MSSA directly on the data, one first finds the MEOFs and uses time-lagged copies of the corresponding PCs in the MSSA, in order to reduce the dimension of the covariance matrix.

We construct a matrix \mathbf{B} whose elements

$$B_{ij} = x_i^{(j)}$$

are the values of the j th variable sampled at time $i\tau_s$, where $i = 1, 2, \dots, N$ and $j = 1, 2, \dots, L$, where each vector $\mathbf{x}^{(j)}$ contains the full time series for a particular variable. The full set of variables might include samples of the same physical variable at different locations and/or different physical variables at the same location(s).

We next subtract from each element of $\mathbf{x}^{(j)}$ the mean value of all its elements, to form a matrix \mathbf{F} consisting of columns $\mathbf{y}^{(j)}$ with zero mean:

$$F_{ij} = y_i^{(j)} = x_i^{(j)} - \frac{1}{N} \sum_{i=1}^N x_i^{(j)}.$$

Since the columns of \mathbf{F} represent different physical variables, we renormalise them so that the results of the analysis are not influenced by the units in which we choose to measure them (Mote et al., 2000). Our data consists of measurements of the bathymetry at 1125 separate locations over Duck beach (covering the area between $y = -91$ to 1097 m along the shore and between $x = 80$ to 520 m offshore), together with measurements of the monthly mean water levels (MWL) and monthly wave heights (MWH) at a wave gauge located near Duck beach, and a measurement of the North Atlantic Oscillation (NAO) spatially averaged over the whole surveyed area, the NAO being the pressure difference between Iceland and the Azores. Since all of these forcings were simultaneously available for only the last 19 years of bathymetric surveys, we reduced the analysis to this duration. We considered two possible choices for the renormalisation factor: the range of each variable or its standard deviation. We decided to use the range because we were interested

in understanding the effect of each possible forcing independently, and using the range separated these out in the calculated MEOFs to a greater degree than using the standard deviation. Finally, since we have 1125 pieces of data for the bathymetry at each time $i\tau_s$ and only one piece for each possible forcing, we divide the bathymetry measurements by 1125 so that the effect of the potential forcings is comparable with that of the spatial variations in the bathymetry. From now on we consider \mathbf{F} to have been renormalised in this manner.

Next, a singular value decomposition (SVD) of \mathbf{F} permits the identification of bathymetric locations where the bathymetry may be strongly correlated with each of the potential forcings. Such decomposition is of the form

$$\mathbf{F} = \mathbf{U}\mathbf{S}\mathbf{V}^T,$$

where the columns of \mathbf{V} are the EOFs of the SVD, or the spatial eigenvectors, the columns of \mathbf{U} are the PCs, or the temporal eigenvectors and \mathbf{S} is the diagonal matrix of eigenvalues; the ratio of each eigenvalue divided by the sum of all the eigenvalues gives the fraction of the total variance explained by each eigenvector. The EOFs represent the stationary patterns in the bathymetry and potential forcings that explain most of the observed variability, with the greatest variance being resolved by the EOF corresponding to the largest eigenvalue and so on. The PCs provide the variation over time of the sign and amplitude of the associated EOF.

Each spatial eigenvector giving a direction in which each potential forcing is dominant gives an excellent proxy of the relative correlation of that phenomenon with that particular spatial mode of the bathymetry. In fact, computing the correlations directly from the data and comparing the correlation distributions to the spatial EOF contours would show that correlation contours and EOF contours are equivalent. This is because of the dominance of the phenomena along well defined EOF directions. Since linear correlations are conceptually more straightforward than EOF distributions, we present and discuss the correlation plots instead of the EOF distributions. However, we use MEOF as a filter for the MSSA.

A.3. MEEOF/MSSA

Multivariate Extended Empirical Orthogonal Functions (MEEOF) is the name given to Multichannel Singular Spectrum Analysis (MSSA) when several different physical variables are included in the analysis. Such a technique

has been useful, in particular, in the analysis of the behaviour of climatic phenomena, with the aim of extracting modulated oscillations from the coloured noise commonly present in natural systems (Vautard and Ghil, 1989; Mote et al., 2000). Its use has focused on accurate identification and characterisation of the system’s temporal and spectral properties. MSSA is fully described in Allen and Robertson (1996) and references therein. Here a short description is presented for the reader interested in the methodology and its capabilities.

Suppose we have the dataset, $\{y_i^{(j)}; i = 1, \dots, N, j = 1, \dots, L\}$, discussed in the previous section. Several techniques to produce a matrix of time-lagged vectors may be proposed. Here the method used by Allen and Robertson (1996) is adopted. It consists of creating the matrices $\tilde{\mathbf{Y}}^{(j)}$, formed by setting the channel to j , $1 \leq j \leq L$, sliding a vector of length M down from $i = 1$ to $i = N' \equiv N - M + 1$ and ordering the resulting vectors from left to right as the columns of $\tilde{\mathbf{Y}}^{(j)}$. Thus each $\tilde{\mathbf{Y}}^{(j)}$ has size $M \times N'$. This leads to a *trajectory matrix*,

$$\tilde{\mathbf{Y}} = \begin{pmatrix} \tilde{\mathbf{Y}}^{(1)} \\ \vdots \\ \tilde{\mathbf{Y}}^{(L)} \end{pmatrix} \quad (4)$$

of size $ML \times N'$.

A singular value decomposition of $\tilde{\mathbf{Y}}$ may then be performed, such that

$$\tilde{\mathbf{Y}} = \mathbf{P}_{\tilde{\mathbf{Y}}} \mathbf{\Lambda}_{\tilde{\mathbf{Y}}}^{1/2} \mathbf{E}_{\tilde{\mathbf{Y}}}^T, \quad (5)$$

where $\mathbf{P}_{\tilde{\mathbf{Y}}}$ consists of the temporal principal components (T-PCs). As equation 5 implies, these are the left-singular vectors of $\tilde{\mathbf{Y}}$. The matrix $\mathbf{E}_{\tilde{\mathbf{Y}}}$ consists of the spatio-temporal empirical orthogonal functions (ST-EOFs) corresponding to the right-singular vectors of $\tilde{\mathbf{Y}}$. Finally, $\mathbf{\Lambda}_{\tilde{\mathbf{Y}}}$ is the diagonal matrix of variances associated with these orthogonal bases (Robertson, 1996).

The bases $\mathbf{P}_{\tilde{\mathbf{Y}}}$ and $\mathbf{E}_{\tilde{\mathbf{Y}}}$ are the eigenvectors of the covariance matrices

$$\mathbf{C}_{\tilde{\mathbf{Y}}}^P = \frac{1}{ML} \tilde{\mathbf{Y}} \tilde{\mathbf{Y}}^T \text{ and } \mathbf{C}_{\tilde{\mathbf{Y}}}^E = \frac{1}{N'} \tilde{\mathbf{Y}}^T \tilde{\mathbf{Y}}, \quad (6)$$

respectively. However, it is only for the smallest of $\mathbf{C}_{\tilde{\mathbf{Y}}}^P$ and $\mathbf{C}_{\tilde{\mathbf{Y}}}^E$ that either $\mathbf{P}_{\tilde{\mathbf{Y}}}$ or $\mathbf{E}_{\tilde{\mathbf{Y}}}$ is full-rank (Allen and Robertson, 1996; Robertson, 1996). Therefore, the choice of M determines which of the eigenbases is to be analysed.

However, the method of construction of $\tilde{\mathbf{Y}}$ implies that the column vectors of $\tilde{\mathbf{Y}}^T$ are time-lagged copies at a given channel, so it is convenient to choose N' small enough to satisfy $N' < ML$, so that the full rank matrix is $\mathbf{C}_{\tilde{\mathbf{Y}}}^E$.

As mentioned in Sect. A.2, rather than performing the MSSA over the data and having to resolve a very large covariance problem, it is better to perform a data reduction procedure by prefiltering the original data with the MEOF and apply the MSSA to the resulting EOFs. In this way, the most important information is compressed into a small number of variables (Plaut and Vautard, 1994) and the analysis of the coherent patterns is simplified significantly. In this case the first three eigenvalues of the MEOF resolve most of the variance and also are the ones in the directions of the three potential forcings considered, so the MSSA can be applied to these three eigenfunctions rather than to the data.

The first 14 MSSA components of the filtered system – that is, the system consisting of the first 3 MEOF PCs as input channels, were analysed. Each of these components has its corresponding eigenvalue, spatiotemporal PC (ST-PC) and spatiotemporal EOF (ST-EOF). A window length of $M = 120$, equivalent to $N' = 9$ years, was chosen. The criteria presented by Plaut and Vautard (1994) were used to identify coherent patterns within the ST-PCs. The method consists of finding pairs of consecutive eigenvalues $(k, k + 1)$ for which:

- the two eigenvalues are nearly equal, that is they are both within the margins of error identified by North’s rule of thumb (North et al., 1982),
- the two corresponding time sequences described by the ST-PCs are nearly periodic, with the same period and in quadrature,
- the associated ST-EOFs are in quadrature and
- the lag correlation between ST-EOFs of order k and $k + 1$ itself shows oscillatory behaviour (Ghil and Mo, 1991).

Pairs that pass all these tests are associated with quasi-oscillations with periods equal to the period of the ST-PCs - which is also the period of the ST-EOFs - in the embedding space, here spanning 121 months.

The first test was to inspect pairs of consecutive eigenvalues $\lambda(k), \lambda(k + 1)$ to see if they satisfied North’s rule of thumb. It was found that eigenvalue $\lambda(k + 1)$ lies within the interval $[\lambda(k)(1 - \sqrt{2/N}); \lambda(k)(1 + \sqrt{2/N})]$, with

$N = 228$ months being the sampling duration, for all pairs considered, so the 7 of them satisfy the first criterion. Then plots of the ST-PCs for the 14 MSSA components at channel 1 showed that all pairs considered are quasi-periodic with same period and in phase quadrature so they also satisfy the second criterion. This led to a check of the quadrature criterion for the ST-EOFs associated with each ST-PC pair. Since the ST-EOFs are the same for all the PCA channels in the prefiltering, only the results for channel 1 are necessary. The ST-EOF plots are shown in Fig. 7 for the first 6 pairs, with the solid line corresponding to the eigenvector with smaller index. All the pairs (including pair 13-14, not shown) pass the test. The final test consists of analysing the lagged correlation plots for the pairs which have satisfied all previous tests. The plots, shown in Fig. 8, should depict oscillatory functions. Again, all pairs pass this test.

Figure Captions:

Caption 1: Data contours for transects 58 (top, North of the pier) and 190 (bottom, South of the pier) with: beach elevation (in metres) displayed in Figs. (a,i) and (b,i); trend signal elevation (in metres) displayed in Figs. (a,ii) and (b,ii) and; detrended signal elevation (in meters) displayed in Figs. (a,iii) and (b,iii). The upper panels in Figs. (a,ii), (a,iii), (b,ii) and (b,iii) show the percentage of variance resolved by the corresponding signal.

Caption 2: Quasi-oscillations identified within the trend (left) and the detrended (right) signals together with the resolved variance, at window lengths of 9 years, for transects 58 (top) and 190 (bottom).

Caption 3: Spectral density plot for the reconstructed component of the SPOs at $x = 160$ m for Transect 58. The thin lines indicate the 95% confidence interval for the spectral estimates.

Caption 4: SSA reconstruction of wave dynamics, with the first fundamental pair shown at the top and the second fundamental pair shown at the bottom.

Caption 5: Correlation Contours between the seabed and the NAO, the MWH and the MWL, respectively. Tr. 58 (top, Northern side) and Tr. 190 (bottom, Southern side), are highlighted (solid lines). The pier is located at $y = 513$ m (dashed line).

Caption 6: First six pairs of ST-EOFs of the MSSA components linked to potentially quasi-oscillatory pairs at all channels, with their associated resolved variance. The abscissa represents time (in months) and spans the window length $M = 121$ months.

Caption 7: ST-PCs for consecutive MSSA components at channel 1; the ST-PCs span the window length $N' = 108$ months.

Caption 8: Lagged correlations for all ST-PC pairs.

Figures:

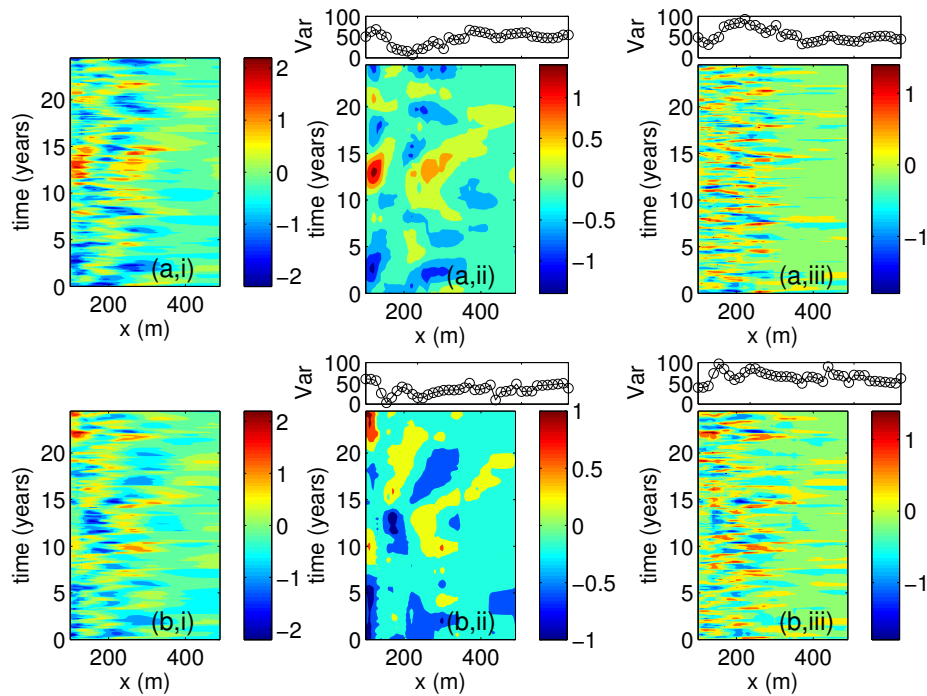


Figure 1: Data contours for transects 58 (top, North of the pier) and 190 (bottom, South of the pier) with: beach elevation (in metres) displayed in Figs. (a,i) and (b,i); trend signal elevation (in metres) displayed in Figs. (a,ii) and (b,ii) and; detrended signal elevation (in meters) displayed in Figs. (a,iii) and (b,iii). The upper panels in Figs. (a,ii), (a,iii), (b,ii) and (b,iii) show the percentage of variance resolved by the corresponding signal.

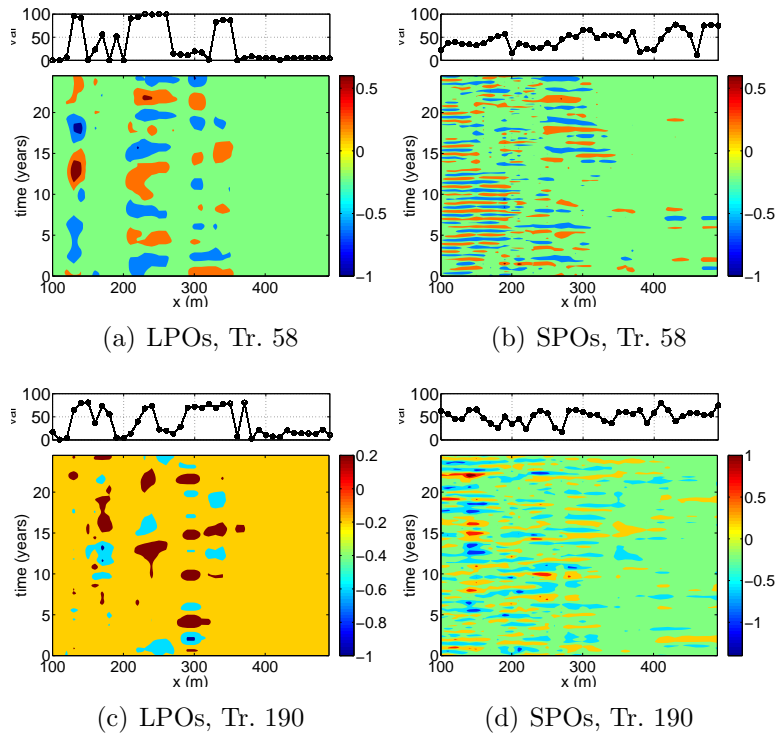


Figure 2: Quasi-oscillations identified within the trend (left) and the detrended (right) signals together with the resolved variance, at window lengths of 9 years, for transects 58 (top) and 190 (bottom).

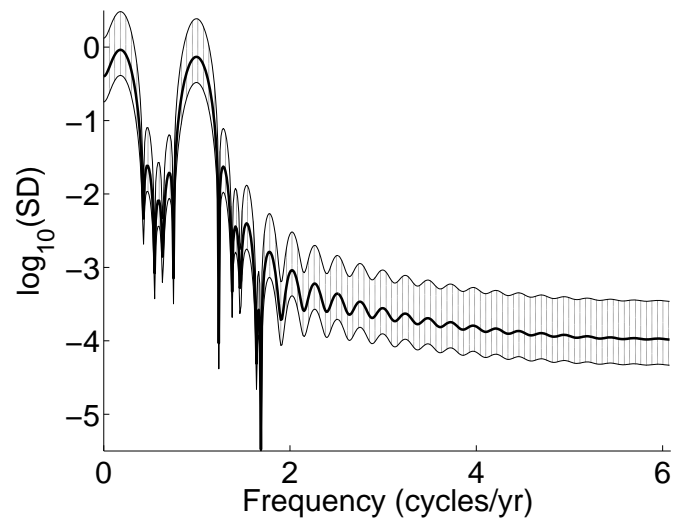


Figure 3: Spectral density plot for the reconstructed component of the SPOs at $x = 160$ m for Transect 58. The thin lines indicate the 95% confidence interval for the spectral estimates.

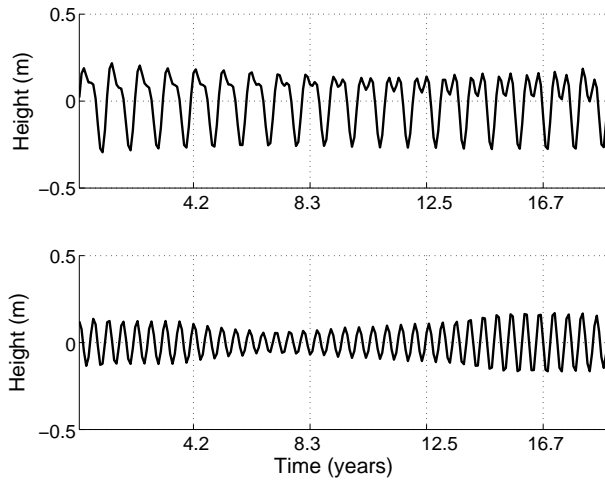


Figure 4: SSA reconstruction of wave dynamics, with the first fundamental pair shown at the top and the second fundamental pair shown at the bottom.

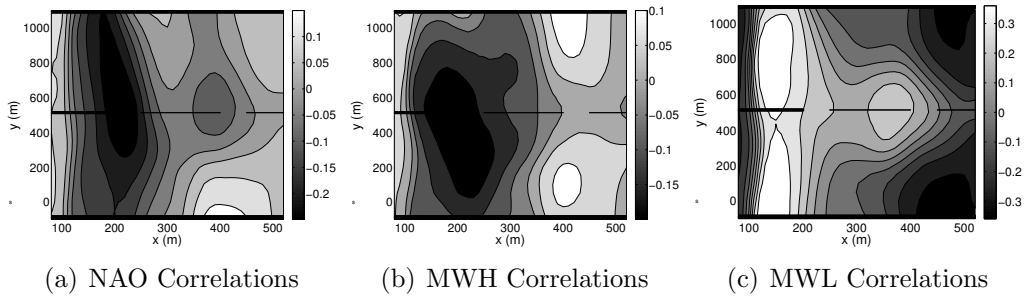


Figure 5: Correlation Contours between the seabed and the NAO, the MWH and the MWL, respectively. Tr. 58 (top, Northern side) and Tr. 190 (bottom, Southern side), are highlighted (solid lines). The pier is located at $y = 513$ m (dashed line).

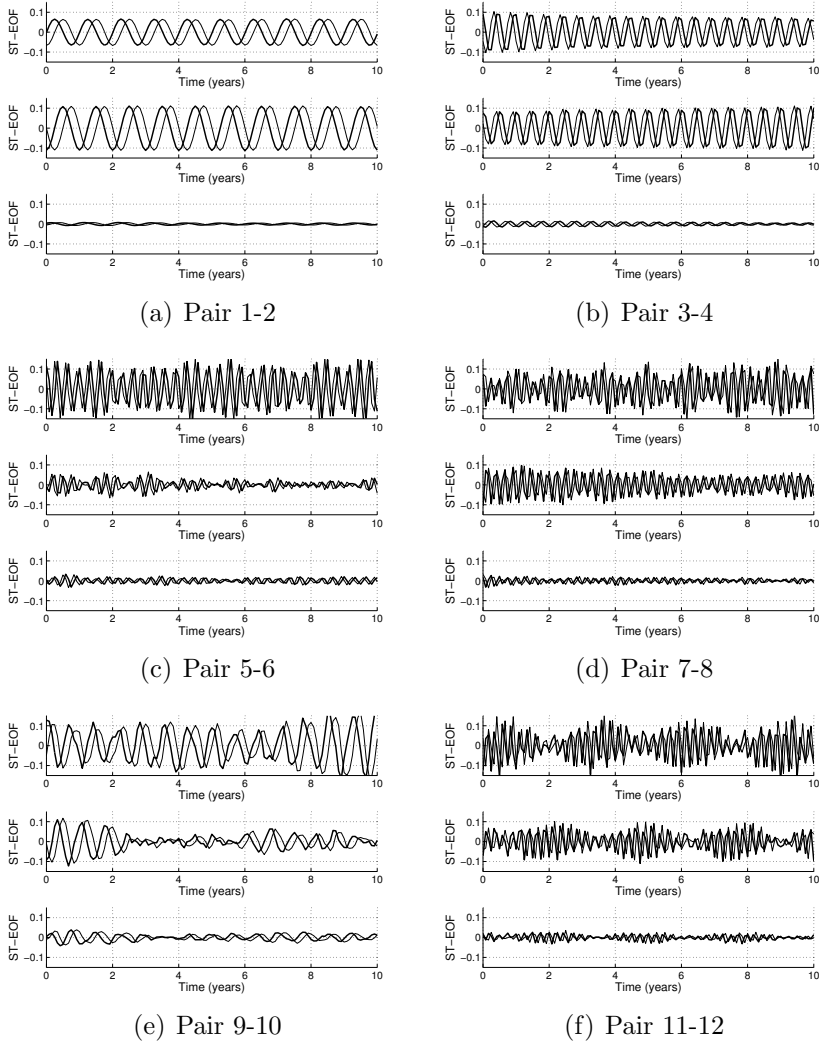


Figure 6: First six pairs of ST-EOFs of the MSSA components linked to potentially quasi-oscillatory pairs at all channels, with their associated resolved variance. The abscissa represents time (in months) and spans the window length $M = 121$ months.

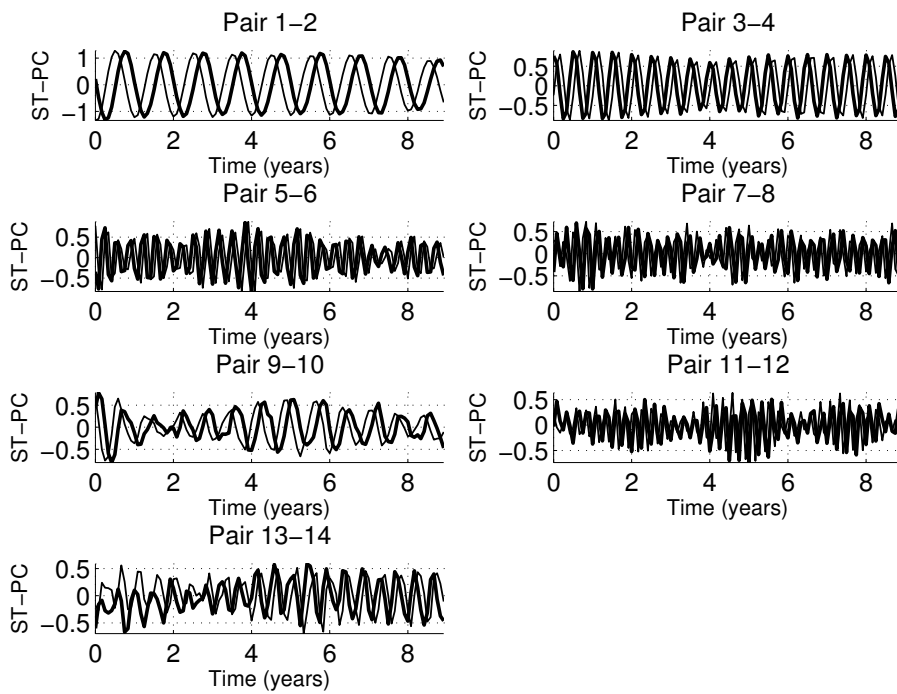


Figure 7: ST-PCs for consecutive MSSA components at channel 1; the ST-PCs span the window length $N' = 108$ months.

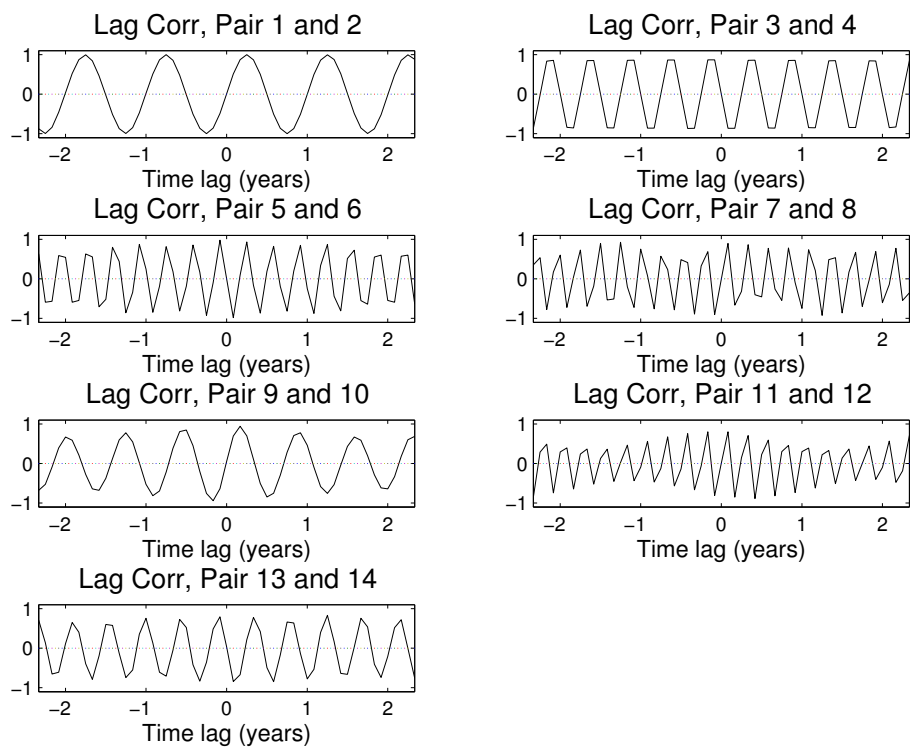


Figure 8: Lagged correlations for all ST-PC pairs.

Tables:

TN	190	188	62	58
\bar{y}	-91	0	1008	1097
Δy	32	17	98	91

Table 1: Correspondence between transect number and transect longshore position for the four best surveyed transects at Duck, North Carolina, USA. TN is the transect number, \bar{y} the averaged longshore position Δy the absolute error around this average.

	Transect 58		Transect 190	
x (m)	LPOs (yrs)	SPOs (yrs)	LPOs (yrs)	SPOs (yrs)
120	6.5(2)	1(0.7)	15.5(1.5)	1(0.1),2.6(0.1)
130	16.4(4)	1(0.1)	8(1)	1(0.1),2.7(0.2)
140	11.4(5.1)	1(0.2)	1.8(0.2),3.1(0.5) 5.6(0.4)	1(0.1),2.4(0.2)
150	3.1(0.6)	1(0.1)	6.5(0.5)	2.1(0.2),1(0.1)
180	3.9(0.3)	1(0.1)	13(1), 1.7(0.1)	2.4(0.2),0.9(0.2)
190	4.7(0.8)	1(0.1)	1.7(0.3)	2.2(0.2),1(0.1)
200	6.4(0.6)	all below 1	5.5(0.2)	2.9(0.5),1.4(0.2),1(0.1)
220	7.9(2.4)	0.8(0.1), 1.8(0.1)	3.6(0.4)	4.4(0.6),1.4(0.2),1(0.1)
230	6.3(1.2)	2.2(0.5)	10(1)	1.5(0.1),1(0.1)
240	4.4(0.8)	1(0.1),1.9(0.2)	12(1)	2.9(0.5)
250	5.4(0.9)	1(0.2),1.8(0.1)	12(1)	2.6(0.3),1.6(0.3),1(0.2)
260	5.2(0.7)	1.8(0.2),4.2(0.6)	14(2)	2.5(0.3),1.6(0.3),1.2(0.2)
310	5.8(0.7)	1.1(0.1),1.7(0.3)	5.8(0.2)	1.2(0.2),1.6(0.3),2.5(0.3)
340	7.3(1.8)	1.5(0.3)	6.5(0.5)	3.1(0.4),1.5(0.3),1(0.2)
350	9.8(4)	2.1(0.9)	6.5(0.5),8(0.4)	1(0.2),1.5(0.2),2.2(0.1)
370	3.4(0.5)	1.4(0.1), 4.8(1.1)	6.2(0.4),9.3(0.6)	1(0.5),2.2(0.2)
390	3.4(0.2)	2.2(0.6)	5.8(0.4)	1(0.5),1.6(0.5),2.3(0.2)
410	3.3(0.9)	1.4(0.1)	4.3(0.2)	1(0.1),2(0.2),3.2(0.6)
470	6.7(0.8)	2.5(0.9)	3.2(0.2),4.8(0.2)	same as 410
480	10.3(6.2)	2.6(0.6),3.3(0.8)	3.3(0.2)	same as 410
490	7.1(2)	2.5(0.5)	4.8(0.2)	1(0.1),1.3(0.4),3.4(0.6)

Table 2: Periods of dominant oscillatory patterns at selected locations along transects 58 and 190, with the uncertainty or confidence interval in brackets.

EOF values with all seabed surveys				
Forcing:	EOF1	EOF2	EOF3	EOF4
NAO	0.998	-0.067	-0.012	-0.0005
MWH	0.067	0.998	0.0005	-0.0009
MWL	-0.012	0.001	-0.999	0.044
EOF values with Transects 58 and 190 only				
Forcing:	EOF1	EOF2	EOF3	EOF4
NAO	0.998	-0.067	-0.013	-0.0001
MWH	0.067	0.998	0.0004	0.003
MWL	-0.012	0.001	-0.940	-0.335

Table 3: Table of components of V associated with the first 4 main SVD components, for the 3 potential forcings considered: the North Atlantic Oscillation (NAO), Monthly-averaged Wave Heights (MWH), and the monthly mean water level (MWL). The forcings have been arranged so that the largest elements in the Forcings/EOFs matrix are in the diagonal.